Novel Methods for Optical Trapping and Raman Spectroscopy of Nanoparticles

by

Behnam Khosravi

B.Sc., Khajeh Nasir Toosi University of Technology, 2014

M.Sc., Shahid Beheshti University, 2017

A Dissertation Submitted in Partial Fulfillment of the

Requirements for the Degree of

Doctor of Philosophy

in the Department of Electrical and Computer Engineering

Novel Methods for Optical Trapping and Raman Spectroscopy of Nanoparticles

by

Behnam Khosravi

B.Sc., Khajeh Nasir Toosi University of Technology, 2014

M.Sc., Shahid Beheshti University, 2017

Supervisory Committee

Dr. Reuven Gordon, Supervisor

(Department of Electrical and Computer Engineering)

Dr. Levi Smith, Departmental Member

(Department of Electrical and Computer Engineering)

Dr. Peter Loock, Outside Member

(Department of Chemistry)

Abstract

This dissertation explores advanced novel techniques in optical trapping and Raman spectroscopy, focusing on the utilization of double-nanohole (DNH) apertures. We investigate polarization selective reflection mode optical trapping, which enhances the precision and efficiency of nanoparticle manipulation compared to conventional transmission mode optical trapping. These studies investigated Raman spectroscopy with DNH trapping, demonstrating significant Raman signal enhancement due to the intense electric fields generated within the DNH gaps. This enhancement is quantified through Raman signal enhancement by using DNHs and providing insights into the mechanisms driving this phenomenon.

Additionally, we present methodologies for observing trapping in real-time using the camera in optical tweezer systems, enabling direct visualization and analysis of the trapping event.

Complementary to the experimental work, DNH simulations are conducted to model the optical and plasmonic properties of the DNH structures. These simulations offered a theoretical framework that supports and explains the experimental findings.

The integration of these techniques not only advances the field of optical trapping and Raman spectroscopy but also creates new opportunities for applications in nanotechnology and materials science.

Contents

List of Figures

ACKNOWLEDGEMENTS

I would like to thank:

my supervisor, Dr. Reuven Gordon, for his invaluable support and insight throughout my studies.

my colleagues in the Nanoplasmonics Research Group, for their support and encouragement, including Ghazal Hajisalem, Michael Dobinson, Ryan Peck, Elham Hosseini, Demelza Wright, Matthew Peters, and Saeid Asadi.

I would like to acknowledge the assistance of Microsoft Copilot while writing my dissertation. The use of this AI model helped me generate and edit content, fix grammatical errors and choose better words for the context. It is important to note that all information provided by Microsoft Copilot was thoroughly reviewed and revised by this author to ensure its accuracy and to make it appropriate for my dissertation.

Dedication

Just hoping this is useful!

Chapter 1

Introduction

This work focuses on the investigation of nano-particles and their Raman emission spectrum. The nano-aperture assisted optical trapping of nano-particles is the basis of this study. Particle detection and identification are major research interests with applications in biomedical [1], environmental [2] and quantum fields [3]. The ability to isolate and investigate a single nano-particle can be helpful in studying its characteristic properties. It has been shown that optical trapping is an effective method for this purpose [4, 5]. By collecting the scattered light from the trapped particle, researchers can analyze the particle's properties, such as its size, shape, and refractive index.

Raman spectroscopy is a widely used analytical technique for detecting and identifying materials, as well as characterizing complex solutions [6]. This method involves shining laser light onto a sample and measuring the scattered light by a spectrometer to obtain a unique spectral data. These data provide detailed information about the molecular composition, structure, and interactions within the sample. Due to its high sensitivity and specificity, Raman spectroscopy is employed in various fields, including chemistry [7], materials science [8], biology [9], and medicine [10]. It is used to

analyze different materials such as pharmaceuticals [11] and nanomaterials [12].

1.1 Reflection Mode Optical Trapping

Optical trapping is a technique that has been used for years to control and monitor small particles at micro or nanoscale [13]. In this method, a focused laser beam will create a strong electromagnetic field on a spot. When laser photons hit a particle, their momentum will change. This change will create a force on the particle that will push it towards the center of the focused laser beam. This will position the particle at the desired location and create conditions for the particle to scatter light. Since the particle is in the focused beam area, the scattered light from the particle can be collected. This way we can have an isolated particle and its scattering characteristics.

A challenge in using the focused laser is that by using a microscope objective, the beam spot diameter depends on the objective that is used. Also, the diffraction limit can affect the particle's interaction with the light and our ability to measure the particle's emissions. As the target particle gets smaller compared to the laser wavelength, the measurement will become harder, until it becomes impossible to observe any scattering from the particle. At this point, aperture assisted optical trapping can be useful [14].

Subwavelength apertures, when combined with surface plasmons, can significantly enhance the electromagnetic field at the nanoscale [15]. This field enhancement is crucial for optical trapping, where nanoparticles can be precisely manipulated and held in place. The interaction between the focused light and the surface plasmons can be more profound at these apertures due to the highly localized field, enabling more efficient trapping and study of nanoparticles [16]. The use of subwavelength apertures and surface plasmons opens up new possibilities in optical trapping because

of their ability to enhance and localize the light in nanoscale dimensions [15].

After using a nano-aperture such as a DNH and trapping a nanoparticle, the transmitted light can be collected. This light that passed through the aperture and the particle, has information about the particle and its dynamics. Rayleigh and Raman scatterings can be detected with this method to gain information from the particle [17]. Various light interactions by quantum dots [18] and nanocrystals [19] and characteristics of bio-molecules [20] can be measured.

This light collection has limitations that will hinder its applications in some areas. The use of two closely spaced microscope objectives, positioned on either side of the sample, makes it difficult to implement more complex experiments. Every component of the sample should be confined in a thin layer and its placement takes time and precision. To mitigate these issues, we can remove the collection objective lens and only use one objective lens on the sample. This objective lens will focus the laser and collect the scattered light from the sample. This will increase the efficiency of detection and makes the optical setup simpler.

To improve the reflection light collection, we used a polarization separation technique. When the incident and reflected lights on the sample are in the same path and have different polarizations, a polarizing beam splitter can be used to separate the reflected light from the incident laser beam. When the incident laser on a DNH is linearly polarized and the laser polarization angle is at 45° compared to the long axis of the DNH, the reflected light polarization will be different than the laser and it is at 90° in comparison to the laser polarization. Using a polarizing beam-splitter one can direct these two beams in different paths and the reflected light can be measured accurately.

This proposed method enables highly accurate measurements of nanoparticle characteristics while eliminating the scattered light from the particle's surrounding

medium. Not only will the utilization of the optical setup be easier, but the accuracy will also improve. This will enable faster experiments and make previously impossible measurements possible.

1.2 Raman Spectroscopy

Raman spectroscopy is widely used for the characterization of nanoparticles [21–23]. This method allows identifying materials by measuring the emitted light from the material while its molecular resonances are being excited by a laser. Conventional Raman spectroscopy employs a spectrometer to detect peaks in the emission spectrum at wavelengths longer than the incident laser.

In addition to conventional Raman spectroscopy, advanced techniques such as Surface-Enhanced Raman Spectroscopy (SERS) [24] and Tip-Enhanced Raman Spectroscopy (TERS) [25] have been developed. These techniques significantly enhance the Raman signal, allowing for the detection of nanoparticles and single molecules and providing detailed information about the chemical composition, structure, and interactions of nanoparticles.

SERS utilizes metallic nanostructures to create a strong electric field and amplify the Raman scattering signal, making it highly sensitive and suitable for detecting low concentrations of nanoparticles. TERS, on the other hand, combines the principles of Raman spectroscopy with scanning probe microscopy, offering high spatial resolution and the ability to study nanoscale features.

These advancements and techniques in Raman spectroscopy have made it an essential tool in nanomaterials science, enabling researchers to explore the properties and behaviors of nanoparticles with unprecedented detail and accuracy.

The challenge of measuring Raman spectrum from individual nanoparticles is that

it requires isolating the nanoparticle and enhancing its signal. A single nanoparticle has a small scattering cross section and its emission is too weak for reliable detection. Past works have used optical trapping with nanoapertures in metal films to enhance and measure the Raman spectra of individual nanoparticles [17, 26]. In those works, custom optical tweezer systems had been used to detect the transmission signal from the aperture to verify the trapping events. Most nanoaperture fabrications used in previous studies employed top-down nanofabrication techniques, which contribute significantly to the overall expense of the measurements.

In this work, Titania nanoparticles were trapped in a commercial Raman system using DNHs and their spectra were measured while the particle is trapped in the aperture. The microscope camera allowed for observing the trapping event in reflection mode, and simultaneously its Raman spectrum was recorded.

Here, the DNHs were fabricated using a colloidal lithography technique, which is cheaper and has high throughput. The DNHs were identified on the gold surface by using a scanning electron microscope, and could be observed on the Raman system camera.

This approach creates a simple way of characterizing individual nanoparticles in a solution using their Raman signal using existing commercial Raman systems. This method can be used for material characterization with low concentrations of nanoparticles in a solution. The recorded Raman signal was comparable in intensity with past work that used a million times larger particles and no DNHs were used [27].

1.3 Contributions

This dissertation demonstrates novel and significant contributions to research on nanoparticle trapping, Raman enhancement, and spectroscopy. The growing need

for molecule-level experiments has created a demand for advanced techniques capable of precise analysis and manipulation of various nanoparticles.

In this work, I have developed an innovative method for optical trapping of nanoparticles, which allows for stable trapping and characterization of particles at the nanoscale. Using a polarization selective setup that detects the reflected light from the aperture and the trapped particle, we can accurately measure the changes in reflection from the particle, which provides insights into the particle's dynamics within the optical trap. This technique can have many applications in various fields, including biophysics and nanotechnology.

Furthermore, I have explored the enhancement of Raman signals by DNHs through SERS. By utilizing subwavelength DNHs, I have achieved significant amplification of Raman signals, enabling the detection of nanoparticles and providing accurate particle fingerprints such as Stokes shifts. This method opens new possibilities for sensitive and specific chemical analysis with simple instruments.

The combination of optical trapping and Raman spectroscopy offers a powerful tool for studying the interactions and dynamics of molecules in real-time. This integrated approach not only enhances the sensitivity and resolution of spectroscopic measurements but also provides new insights into molecular behavior at the nanoscale.

Overall, the contributions presented in this dissertation address critical challenges in nanoparticle manipulation and molecular spectroscopy, paving the way for future research and applications in nanoscience and nanotechnology.

1.3.1 Reflection Mode Optical Trapping Using Polarization Symmetry Breaking from Tilted Double Nanoholes [28]

Behnam Khosravi was responsible for sample fabrication, optical setup preparation, measurements, data analysis and writing the manuscript. Reuven Gordon conceptu-

alized the experiments, offered advice on data analysis, and contributed to writing the manuscript.

1.3.2 Accessible Double Nanohole Raman Tweezer Analysis of Single Nanoparticles [29]

Behnam Khosravi was responsible for sample fabrication, operating the Raman system, data acquisition, data analysis and writing the manuscript. Reuven Gordon conceptualized the experiments, offered advice on data analysis, and contributed to writing the manuscript.

1.3.3 Polarization Selective Reflection Geometry Trapping of Nanoparticles [30]

Reuven Gordon conceptualized the idea. Behnam Khosravi was responsible for experiments.

Chapter 2

Theory and Previous Work

The field of plasmonics has emerged as a way to confine light in sub-wavelength structures to increase light-matter interaction. This will create an opportunity for this field to be used in a wide range of applications. Surface plasmons can be used in communication and sensor applications such as Raman spectroscopy [31], resonance sensors [32, 33], light emitters [34, 35] and amplifiers [36, 37], modulators [38, 39], etc. Their ability to confine light in a small area makes them advantageous compared to conventional dielectric lenses. This will create higher spatial resolution for imaging the electromagnetic wave.

Arrays of holes in metal films have been used extensively to study electromagnetic wave transmission through apertures with diameters smaller that their wavelength. Plasmonic oscillations dominated the transmission of light through small apertures. Unlike Bethe theory [40] which predicted less transmission by shrinking the hole sizes, theoretical and experimental studies show that transmission intensities can increase through specific sized holes forming an array [41].

Surface plasmons are propagating electrical waves on the surface of a metal. In order to confine these waves and achieve high field intensities on the metal, plasmon

oscillations should be limited to sub-wavelength structures. These structures can be arrays of sub-wavelength spheres, rods or more complex geometries and the goal is to achieve the highest efficiency by increasing field intensity and reducing losses in electron oscillations. One of the main advantages of these nano-structures is the correspondence between their resonance frequency and their size. It will allow the fabrication of structures that can interact with specific light frequencies and will resonate in the desired wavelength. By changing the geometry of these nano-structures, high electron density areas can be excited in a certain wavelength and the peak absorption in their spectrum can be manipulated as desired.

The concept of using focused optical waves to create forces that can manipulate nano-particles, was introduced in 1986 [42]. It was used to detect and manipulate small particles that could not be done by conventional chemical and physical methods [43]. A conventional optical tweezer will use a focused laser beam to attract particles to the focus point. The focus point is usually a few hundred nano-meters in diameter, hence the particles need to be larger than 100 nano-meters to have a stable and measurable effect on the laser beam.

Localized surface plasmons can be used to enhance previously reliable methods of light manipulation and detection. One of the interesting applications of localized surface plasmons is to use them in conjunction with optical tweezers. The enhanced field in a plasmonic nano-aperture can increase the performance of optical tweezers and make them more reliable and useful for trapping smaller particles [44].

2.1 Plasmonics

Plasmonics is a rapidly evolving field that bridges the gap between optics and nanotechnology. At its core, plasmonics involves the study of surface plasmons, which

are coherent oscillations of electrons at the interface between a metal and a dielectric. These oscillations are excited by light and are capable of confining electromagnetic energy to dimensions much smaller than the wavelength of light, leading to a host of novel applications and phenomena.

Light-matter interactions can create excitations on different material interfaces. These interfaces can be dielectric to dielectric, dielectric to semiconductor, semiconductor to metal and dielectric to metal. Surface plasmons are oscillations of free electrons at the metal-dielectric interface. They can propagate on the surface of the metal and slowly attenuate as they travel. These propagating waves of electric field, can have a smaller wavelength than the wave exciting them. These traveling dipoles are called surface plasmon polaritons (SPP) [45]. These waves will decay exponentially along the direction of travel as they travel on the metal surface.

At optical frequencies, the permittivity of the dielectric is positive and the permittivity of the metal is negative, thus surface plasmons will propagate on the surface of the metal and create SPPs. These SPPs can propagate through gaps or corrugations of the metal surface if the density of the charges is high [46].

Subwavelength apertures and structures can also enhance SPP intensity and their propagation length [47]. In order to achieve this enhancement, the size of the aperture or periods of the corrugations should be much smaller than the wavelength of the incident beam. Figure 2.1 shows two modes of SPPs and their associated electric field on a corrugated surface. It can be seen that in one mode the field has a minimum between the two structures and has a maximum in the other one. Both of these modes will be excited simultaneously with their intensities adjustable by altering the structure's geometry. In a DNH, mode (A) is similar to the wedge plasmon and mode (B) is similar to the gap plasmon [16].

The unique properties of surface plasmons have led to a wide range of applications

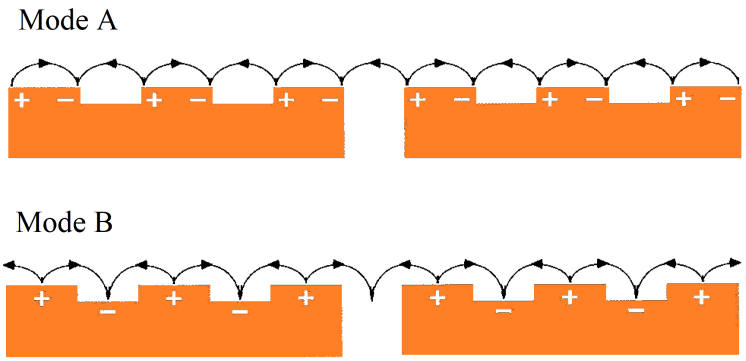

Figure 2.1: Two modes of propagation for surface plasmons on a corrugated surface. Mode (A) is excited due to the sharp edge of the wedge and mode (B) is excited due to the periodic wedge structure.

across multiple fields. Some of the most notable applications include:

- Sensing and Detection: Plasmonic sensors based on surface plasmon resonances (SPR), are highly sensitive to changes on their surface [48]. This makes them useful for detecting biochemical interactions, environmental monitoring, and medical diagnostics. SPR sensors can detect small changes in refractive index. This allows real-time, label-free detection of molecular binding events [49].

- Nanophotonics: Plasmonics enable the manipulation of light at the nanoscale. This leads to the development of compact and efficient optical components. Waveguides, modulators, and switches can be made using plasmonic structures and use them in photonic circuits [50]. This will make high-speed and high-density communication and data processing circuits. Confining light to sub-wavelength dimensions enables high-resolution imaging and lithography.

- Energy Harvesting: Plasmonic nanostructures enhance the absorption of light, making them useful for solar energy harvesting. Concentrating light into small volumes, can increase the efficiency of photovoltaic cells [51] and light sensors.

- Medical Applications: Plasmonic nanoparticles can generate heat when illuminated by light. They can be used in photothermal therapies [52]. In these therapies, they target cancer cells with plasmonic nanoparticles and excite them with light, causing localized heating that destroys the cancer cells without harming surrounding healthy tissue. Plasmonic nanoparticles can also enhance medical imaging techniques.

Noble metals like gold and silver are used extensively in plasmonics. They can support strong surface plasmon resonances. These metals have a high density of free electrons, which is essential for the excitation of surface plasmons. These free electrons can oscillate collectively when interacting with incident light, creating localized

surface plasmon resonances (LSPRs). This results in strong electromagnetic fields at the metal surface.

Moreover, noble metals exhibit relatively low intrinsic electronic losses at optical frequencies, especially compared to other metals [53]. This means that they can support surface plasmon resonances with low energy dissipation, which is important for maintaining strong plasmonic fields and less heat generation.

One of the most important features of noble metals like gold is their chemically inert nature. This makes them the best candidate for use with various chemicals because of their durability. They resist oxidation and corrosion by the sample. This stability helps maintain the performance of the plasmonic nanostructures over time and have consistent measurement results. They can be used in various environmental conditions and applications.

The permittivity of noble metals is such that they exhibit a negative real part and a small positive imaginary part in the visible and near-infrared regions of the spectrum. This makes them suitable for achieving significant field enhancements at these wavelengths especially for Raman spectroscopy. The relative permittivity values of gold for different frequencies are shown in Figure 2.2. Visible frequencies are in the region where real part of permittivity is negative.

The relatively easy fabrication process for noble metals for nanostructures using established nanofabrication techniques such as electron beam lithography, focused ion beam milling, and chemical vapor deposition, helps achieving consistent samples. Gold and silver, in particular, have been shown to produce very strong and sharp plasmonic resonances, which are essential for applications like SERS, biosensing, and nanophotonics [55]. These strong resonances lead to enhanced electromagnetic fields, which significantly improve the sensitivity and efficiency of plasmonic devices.

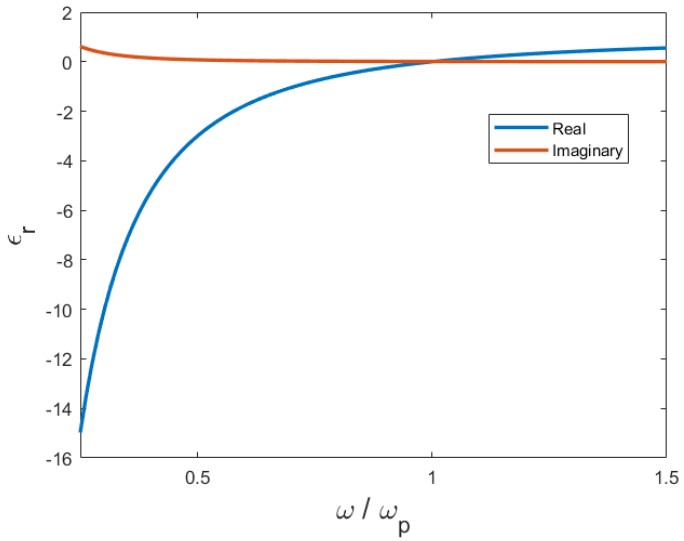

Figure 2.2: Relative permittivity for gold. These values have been calculated using equation 2.1 and data from [54].

2.1.1 Surface Plasmon Excitation

Surface plasmons can be divided into two main types: propagating SPPs and localized surface plasmons (LSPs).

- SPPs are waves that travel along the metal-dielectric interface. Their electromagnetic fields decay exponentially perpendicular to the interface. The confinement of these waves to the surface allows for strong field enhancement at the nanoscale.

- Localized surface plasmons, are confined to metallic nanostructures, such as nanoparticles or nanoholes. These localized modes result in strong electromagnetic fields around the nanostructures, leading to enhanced light-matter interactions. The resonant frequency of LSPs depends on the size, shape, and material properties of the nanostructures, leading to tunable characteristics.

SPPs result from the interaction of light with free electrons at a metal-dielectric interface. These electromagnetic waves propagate along the surface of metals, with their energy confined to the interface, decaying exponentially perpendicular to it. This behavior is particularly interesting due to the sub-wavelength confinement of these waves.

Dielectric constant in a metal depends on the frequency of the incident light and can be determined by equation 2.1. This equation shows the Drude model for relative permittivity of a metal including losses [56].

$$\epsilon_r = 1 - \frac{\omega_p^2}{\omega^2 + i\gamma\omega} \tag{2.1}$$

In this equation ϵ_∞ equals 1, it is representing the metal permittivity as the frequency approaches infinity. ω_p is the plasma frequency and for metals, it is in

the ultra-violet region. At this frequency, the oscillation of electrons on the metal surface are in resonance with the incident light. Any light below this frequency will be reflected unless a sub-wavelength structure creates a different resonance frequency for the light to couple with. To model losses in the plasmonic oscillations, γ is added to the expression as the imaginary part of the relative permittivity. These losses will damp the oscillations of electrons. Part of these losses are caused by scattering of electrons with other electrons or with the metal lattice that creates phonons [57].

Plasma frequency can be determined by equation 2.2:

$$\omega_p = \sqrt{\frac{ne^2}{\epsilon_0 m}} \tag{2.2}$$

where n is the electron density, e is the electron charge, ϵ_0 is the vacuum permittivity, and m is the effective mass of the electron.

These surface plasmons will create an electric field on the surface of the dielectric and the metal. This field will decay rapidly through the material. This means a near field non-radiating wave will be formed by the surface plasmons. Figure 2.3 shows the amplitude of the surface plasmon fields and their exponentially decaying characteristic.

To calculate the momentum of the excited surface plasmons we can use the dispersion relation [58] and it can be seen in equation 2.3:

$$k_{SP} = k_0 \sqrt{\frac{\epsilon_d \epsilon_m}{\epsilon_d + \epsilon_m}} \tag{2.3}$$

in which, k_{SP} is the surface plasmons wave vector, k_0 is the free space photon wave vector of the incident beam and ϵ_d and ϵ_m are the permittivities of the dielectric and the metal, respectively. Because the permittivity of the dielectric is positive and for the metal is negative and has an imaginary part in certain frequencies, k_{SP} will

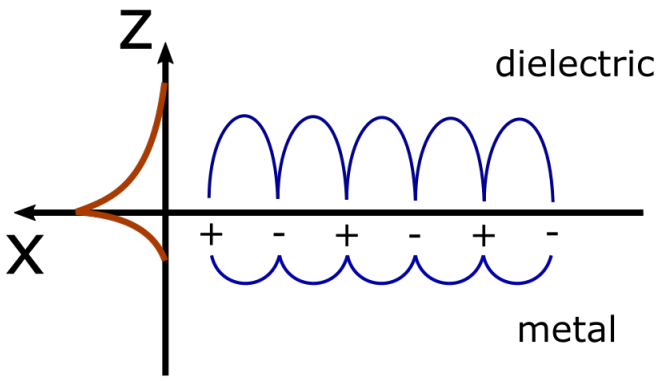

Figure 2.3: The electric field intensity inside the metal and dielectric where surface plasmons are excited. The field decays faster in the metal away from the surface. These surface plasmon polaritons will propagate on the surface away from the light incident point.

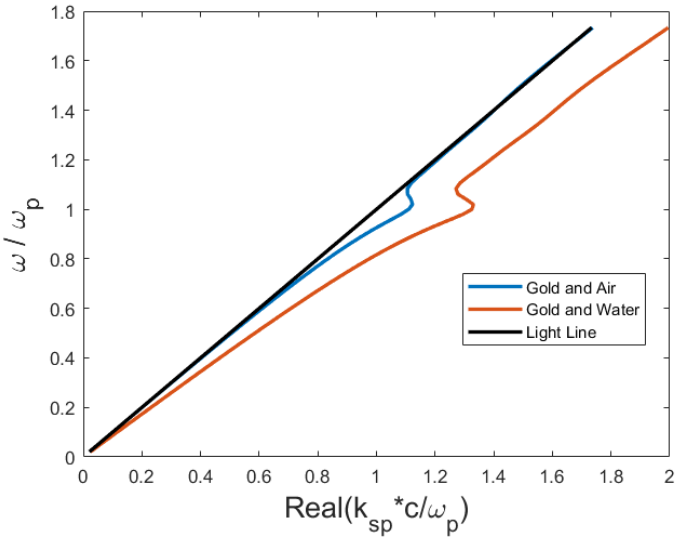

Figure 2.4: Real part of surface plasmons wave vector in different frequencies for gold in contact with air and water. Light line can be seen for reference. The values are divided by the plasmon frequency of gold. Data used from [59].

be greater than k_0 and hence the surface plasmons will be excited. Figure 2.4 shows the dispersion curve for gold interface with air and water compared to the light line.

The momentum of the surface plasmon is greater than the exciting light. To create the extra momentum required to excite surface plasmons, three methods are available. The first method is to use a prism to couple the incident light to the surface plasmons. The two configurations of light coupling are called Kretschmann [60] and Otto configurations [61]. The second method to add momentum is to use subwavelength defects on the surface like nano-antennas or nano-holes to scatter the light and create local surface plasmons. The third method is to use periodic corrugations on the metal surface which have sub-wavelength features [45].

Despite the promising applications, there are several challenges in the practical implementation of SPP-based devices. One of the primary issues is the inherent loss associated with SPP propagation. Metals, while supporting SPPs, have significant absorptions, leading to energy dissipation. Aperture structures can reduce these

losses.

Another challenge is the fabrication of plasmonic nanostructures with precise control over their size, shape, and arrangement. Advances in nanofabrication techniques, such as electron beam lithography and self-assembly, are improving fabrication precision. A colloidal lithography method used in this work is a solution to this challenge.

2.2 Plasmonic Structures

Subwavelength apertures can create localized plasmonic fields with significantly enhanced intensities. When the size of these apertures is much smaller than the wavelength of the incident light, they can support localized surface plasmons (LSPs). This enhancement is particularly strong when the aperture dimensions will cause resonance with the incident light, leading to enhanced field intensity and confinement.

There are several types of plasmonic structures, each with unique properties and applications. Some of the most common structures include:

- Nanoparticles: Metallic nanoparticles, such as gold and silver, can support localized surface plasmon resonances (LSPRs) [62]. These resonances result in strong field enhancement and are highly sensitive to a change in the surrounding dielectric environment. Nanoparticles are widely used in sensing and medical applications [63].

- Nanowires and Nanorods: These elongated structures can support both LSPRs and propagating SPPs. Their shape and aspect ratio allow for tunable plasmonic properties, making them useful in waveguides [64] and optical communications [65].

- Nanoholes and Nanoslits: Arrays of Subwavelength nanoholes or nanoslits in a metallic film can create plasmonic modes that enhance light transmission

through the apertures. These structures are employed in applications like enhanced spectroscopy [66] and light modulation [67].

- Metasurfaces: These are two-dimensional arrays of plasmonic nanostructures that can manipulate light in ways not possible with natural materials [68]. By designing the shape and arrangement of the nanostructures, we can control light propagation, reflection, and refraction.

Factors that can influence the plasmonic properties of these structures include:

- Material Choice: Noble metals like gold and silver are popular choices due to their favorable plasmonic properties [53]. However, other materials like aluminum, copper, and transition metal nitrides are also explored for specific applications [53, 69, 70].

- Geometry and Size: The shape, size, and aspect ratio of plasmonic nanostructures determine their resonance frequency and field enhancement factor. For instance, smaller nanoparticles have higher resonance frequencies [71], while longer structures like nanorods can support multiple resonant modes [72].

- Adjacent dielectric: The surrounding dielectric material impacts the resonance frequency of plasmonic structures [58]. Changes in the refractive index near the metal surface can shift the plasmonic resonance. This makes these structures highly sensitive to the changes in their surrounding medium [73, 74].

2.2.1 Applications

The main feature of plasmonic structures is their ability to concentrate electromagnetic fields into small volumes. This concentration of light results in enhanced light-matter interaction, enabling many applications.

This unique property of nano-scale plasmonic structures improves the performance of many devices across various fields. Some of the most prominent fields of applications include:

Sensing and Detection:

Plasmonic structures are highly sensitive to changes in their surrounding medium. This makes them good candidates for sensing applications. Surface plasmon resonance (SPR) sensors rely on the excitation of surface plasmons at a metal-dielectric interface and can detect small changes in refractive index of the dielectric. They can be used for the detection of biomolecular interactions [49]. Localized surface plasmon resonance (LSPR) sensors use nanoparticles and can achieve high sensitivity. The strong field enhancement around the nanoparticles amplifies the signals from molecules [75].

Imaging and Spectroscopy:

The strong field enhancement in subwavelength plasmonic structures can be used for imaging and spectroscopy. Techniques like SERS benefit from the amplified electromagnetic field around plasmonic structures [76]. It will increase their signal intensity and improve their detection sensitivity. In imaging applications, plasmonic structures can be used to achieve high resolution images beyond the diffraction limit. Techniques like plasmonic nanoscopy use the confinement of light by plasmonic nanostructures to achieve high resolution images of small samples [77].

Photothermal Therapy:

Plasmonic nanoparticles can convert absorbed light into heat, a property that can be used in photothermal therapy (PTT) for cancer treatment. By loading cancer cells with plasmonic nanoparticles and using near-infrared light to excite LSPs, localized

heating leads to the destruction of cancer cells [52].

Energy Harvesting:

Plasmonic structures can increase the absorption of light in photovoltaic devices and improve their efficiency. These nanostructures can increase the generation of charge carriers, leading to higher current density [51].

Communications:

Plasmonic waveguides and circuits enable the manipulation and transmission of light at the nanoscale, enabling high-speed and high-density optical communication systems. Plasmonic devices, such as modulators and switches, can operate at faster speeds compared to conventional electronic devices [38, 39].

2.2.2 Challenges

Despite great promises of subwavelength plasmonic structures, there are several challenges in realizing their potential.

Metals used in plasmonic structures exhibit significant absorption losses, which can limit the efficiency and propagation length of surface plasmons. Exploring alternative materials with lower losses, such as transition metal nitrides, and hybrid metal-dielectric structures might help mitigating this issue.

Precise fabrication of plasmonic nanostructures is challenging. Inaccuracies in their dimensions and arrangements affect their performance. Advances in nanofabrication techniques, such as electron beam lithography, focused ion beam milling, and self-assembly, are making it easier to achieve high-quality plasmonic structures.

Plasmonic nano-devices are usually fixed in place and cannot be changed after fabrication. Developing active plasmonic devices that can be dynamically controlled

using external stimuli, such as electrical, thermal, or optical fields is useful for many applications. These devices would enable reconfigurable plasmonic components.

2.2.3 Conclusion

Plasmonic nano-structures are advancing and have the potential to change various technologies. By utilizing localized surface plasmons, improvements in sensing, imaging, therapy, energy harvesting, and communications can be achieved. As fabrication techniques improve and new materials are employed, application of plasmonic nanostructures will expand and drive progress in science and engineering.

2.3 Double-Nanohole Structure

As stated before, one way to excite surface plasmons is to use defects on the metal surface. One type of defect is to create sub-wavelength apertures. In this work DNHs where used as the plasmonic structure. This structure consists of two touching holes in a metal. DNHs have been extensively used for plasmon excitations [16, 49, 78, 79]. The nano-scale gap between the holes in a DNH will create a plasmonic resonance that enhances the electrical field induced by the laser. This enhancement can be used to trap and amplify the characteristics of materials.

DNHs are an interesting type of plasmonic nanostructures that consist of two closely spaced nanoscale apertures in a metallic film. These structures have attracted significant attention due to their ability to confine light to extremely small volumes, leading to enhanced light-matter interactions. This section delves into the principles, fabrication, and applications of DNHs.

DNHs utilize the phenomenon of LSPRs to achieve sub-wavelength confinement of light. When light interacts with the metallic film with DNHs, it excites LSPPs

confined around the aperture and along the metal-dielectric interface. The presence of the two nanoholes creates a localized electromagnetic field enhancement in the gap between the holes, resulting in strong field enhancement.

The field enhancement is influenced by several factors, including the size and spacing of the nanoholes, the orientation of the holes compared to the light polarization, the material properties of the metal, and the wavelength of the incident light. By carefully tailoring these parameters, we can achieve significant field enhancements, making DNHs ideal for applications requiring high sensitivity and resolution.

2.3.1 Fabrication Methods

The fabrication of DNHs involves advanced nanofabrication techniques to achieve precise control over the size, shape, and spacing of the apertures. Some common methods are as follows.

Electron Beam Lithography (EBL) is a high-resolution lithography technique that uses a focused beam of electrons to pattern the metallic film [80,81]. This method allows for the creation of nanoholes with sub-10 nm precision. In this method, two holes are created on the metal in close proximity. This will create a DNH with a gap in the middle.

Focused Ion Beam (FIB) Milling uses a focused beam of ions to etch the metallic film, creating nanoholes with high accuracy [41]. This technique is particularly useful for creating complex nanostructures. In this method one aperture is made at a time and consecutive ones are slightly different than each other.

Nanoimprint Lithography (NIL) is a cost-effective and high-throughput technique that uses a mold to imprint the nanohole pattern onto the metallic film [82,83]. This method is suitable for large-scale production of DNHs.

Colloidal Lithography which was used in this work is a cost effective and fast

fabrication method for mass production of DNHs [84]. In this method, polystyrene DNHs will be used to create holes on the metal film and produce arrays of DNHs on each sample.

2.3.2 Double-Nanohole Simulations

A DNH in a metal film will create plasmonic resonances when an electromagnetic wave hits the surface. The frequency of these resonances can be seen in the transmission spectrum and it depends on the size and shape of the holes and the gap between them. By tailoring its dimensions, the resonance frequencies and peaks in transmission spectrum can be shifted towards the desired frequencies.

These peaks correspond to the wedge and gap plasmonic resonances in the structure [85]. The wedge resonance is created by the sharp point of the metal on each side of the gap and the gap resonance is due to the gap between the two wedges. If a DNH is going to be used in an optical trapping setup for trapping particles, we should have the maximum change in transmission when a particle is being trapped. To achieve this, the laser wavelength should be at an inflection point near the tip of the resonance peak in the transmission spectrum of the DNH. This way, an increase or decrease in the transmission can easily be observed and measured when the particle is trapped.

To investigate the characteristics of DNHs and their light interactions, a series of simulations have been done using Lumerical FDTD. To create the simulation structure, DNHs were created on a gold film between a glass layer and the liquid containing nano-particles. The incident laser beam goes through the glass layer towards the gold layer, creating the Kretschmann configuration to excite plasmonic resonances around the DNHs. Monitors placed on both sides of the DNH to measure the transmission, reflection and electric field profile on the gold.

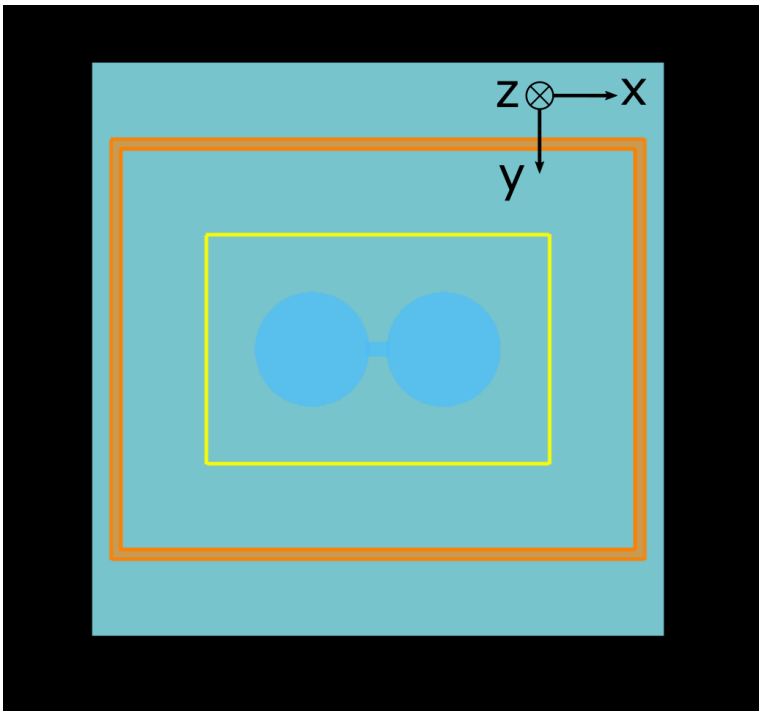

Figure 2.5: Schematic diagram of the simulated DNH structure in Lumerical FDTD. The hole diameter is 400 nm and gap size is 50 nm. The gold layer is 70 nm thick and its between water and air with refractive indices from [86]. The incident beam is in the z direction and its polarization is linear and in the y direction. The yellow rectangle is the incident beam area and the orange rectangle is the FDTD box.

Figure 2.5 shows the simulation structure for a DNH with hole diameter of 400 nm and a gap size of 50 nm. The incident beam is traveling in the z direction and its polarization is linear and in the y direction.

The simulated transmission spectrum for different hole diameters is shown in figure 2.6. The gap for these DNHs was 50 nm. In these simulations, there are peaks in the transmission spectrum that represent resonances between the gaps and along the holes. Because these diameters are large compared to the gap size, resonances along the holes are dominant and resonances along the gaps have smaller peaks. It can be seen that the gap resonances shift slightly by changing the hole diameters. These simulations show that the diameter of the nanoholes can significantly shift the dominant resonance frequency. By choosing a diameter that will have a slope at the

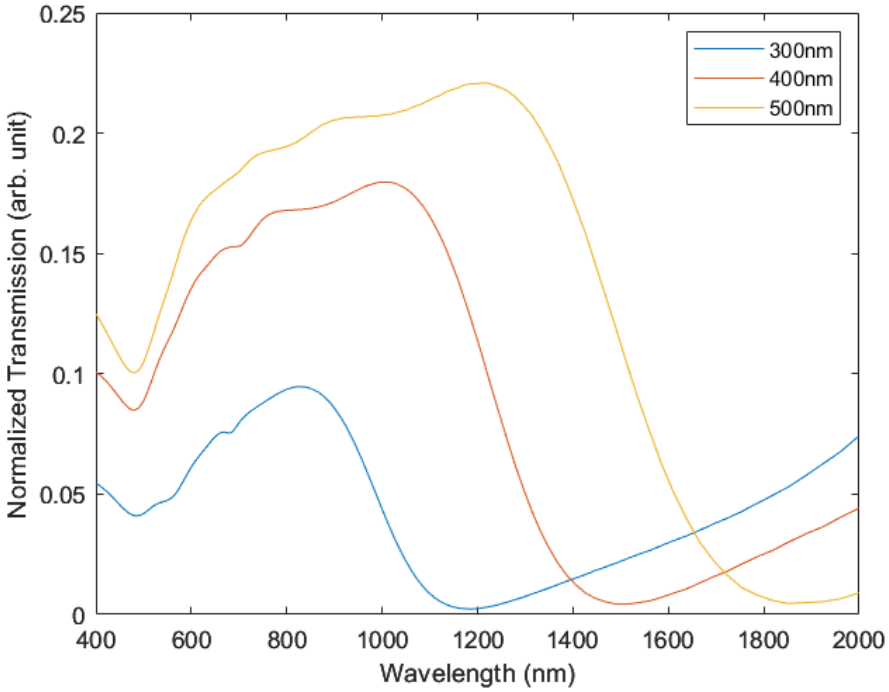

Figure 2.6: Transmission spectrum for three different hole diameters with a fixed gap size of 50 nm. The transmissions are normalized to their respective incident wave intensity.

laser frequency, the change in reflection intensity after trapping, can be larger.

The simulated transmission spectrum for different gap sizes with a fixed hole diameter is shown in figure 2.7. If the hole diameter is larger than 200 nm, the gap size will have a small effect on the resonance peaks. The change in hole plasmon resonance frequency is due to the change in the shape of the holes when the gap is being altered. The hole diameter was 300 nm in these simulations. It can be seen that as the gap size is getting smaller, the transmission intensity at resonance increases.

By changing the geometry of the DNH, the resonance frequency can be close to the desired laser wavelength. Hence, the LSPP can be excited to create high intensity electric fields. The reflection from the DNH can be calculated as 1 minus the transmission due to negligible losses in the simulations. The reflection and transmission

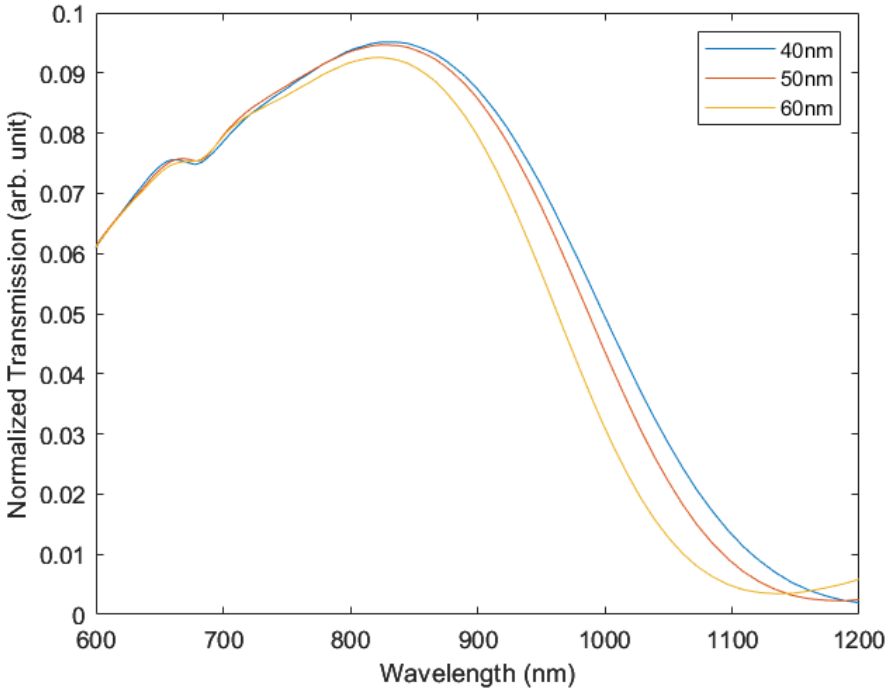

Figure 2.7: Transmission spectrum for three different gap sizes with a fixed hole diameter of 300 nm. The transmissions are normalized to their respective incident wave intensity.

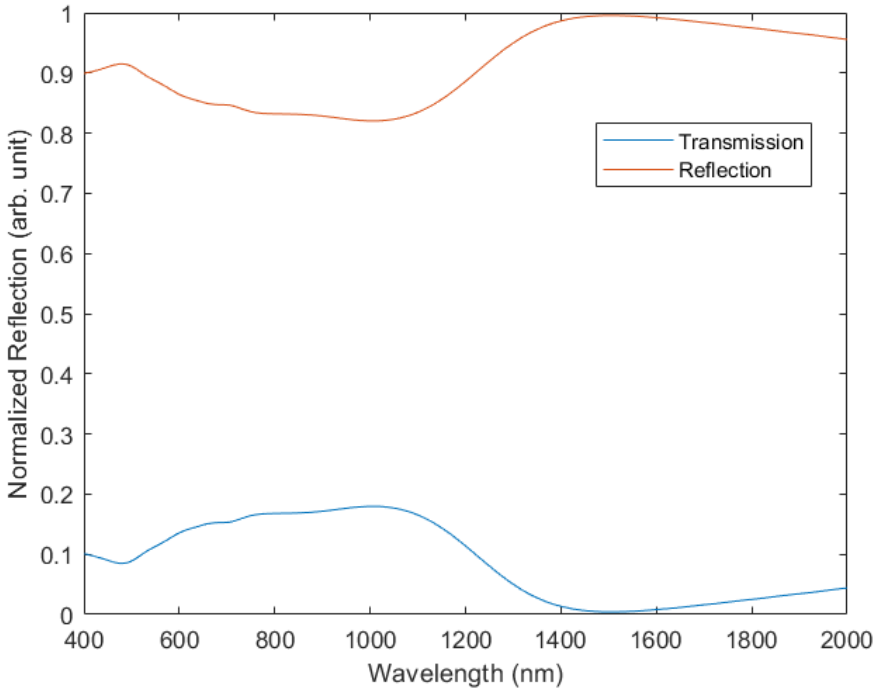

Figure 2.8: Reflection and transmission intensities for a DNH with hole diameter of 400 nm and gap size of 50 nm.

intensities for a DNH are shown in figure 2.8.

This enhanced field from the resonance, will induce a force to trap nano-particles in the gap between the two holes. The reflected laser beam from the DNH can be collected and directed to an Avalanche Photodiode for detection and observation of a change in the plasmonic resonance frequency of the gap in the DNH [28].

2.3.3 Applications of Double Nanoholes

DNHs have a wide range of applications in various fields due to their unique plasmonic properties. In sensing and detection, DNHs are highly sensitive to changes in their local dielectric environment. This makes them ideal for biosensing applications [78]. Sensors based on DNHs can detect biomolecular interactions with high precision and sensitivity [49].

In the field of fluorescence enhancement, the strong electromagnetic fields generated by DNHs can enhance the fluorescence of nearby molecules [16]. This property can be used in fluorescence spectroscopy to achieve high signal-to-noise ratio and improve detection sensitivity.

For optical trapping, DNHs can be used to trap nanoparticles and biological molecules using optical tweezers [87, 88]. The enhanced field intensity allows for the trapping of particles and studying single-molecule dynamics and interactions [49, 89, 90].

2.4 Optical Tweezers and Optical Trapping

Optical tweezers, also known as single-beam gradient force traps, are scientific instruments that use a highly focused laser beam to apply force to particles, such as molecules, nanoparticles, and biological cells, without physical contact. This technology, pioneered by Arthur Ashkin [42], has impacted biophysics, nanotechnology, and materials science.

Optical tweezers are systems that hold a particle in place using optical forces induced on the particle. When a photon hits a particle, it will scatter an its momentum will be affected by the particle. This change in momentum is due to an exchange between the photon and the atoms in the particles. this momentum will create forces that applies to the particle. The main components of these forces are scattering force and gradient force. The gradient force will move the particle in the direction of high photon concentration. By using a microscope objective and focusing a laser beam on a small area, the particles will move toward the focusing point. This phenomenon can be used to manipulate and sense nano-particles [91].

Gradient Force

This is the dominant force in optical tweezers, responsible for trapping the particle [91]. The gradient force arises due to the spatial variation in the intensity of the laser beam. A particle in the beam experiences a force that pushes it towards the region of highest intensity, which is typically at the focal point of the laser. This force can be described by equation 2.4.

$$F_{grad} = -\frac{1}{2}\alpha\nabla|E|^2 \tag{2.4}$$

where α is the polarizability of the particle, ∇ is the gradient operator, and $|E|^2$ is the intensity of the electric field.

Scattering Force

This force results from the scattering of photons by the particle. It acts in the direction of the laser beam's propagation and tends to push the particle out of the trap. The scattering force can be counteracted by adjusting the laser intensity and focal parameters to maintain a stable trap. The scattering force is given by equation 2.5.

$$F_{scat} = \frac{nP}{c}\hat{a}Q \tag{2.5}$$

where n is the refractive index of the surrounding medium, P is the power of the laser beam, c is the speed of light, $\hat{a}$ is the unit vector in the direction of the beam propagation and Q is the scattering efficiency, which depends on the size, shape, and refractive index of the particle, as well as the wavelength of the light.

Figure 2.9 shows the forces that are applied to a particle under focused laser influence. It can be seen that the equilibrium point for forces is near the focus point of the laser and the particle will be held in that location.

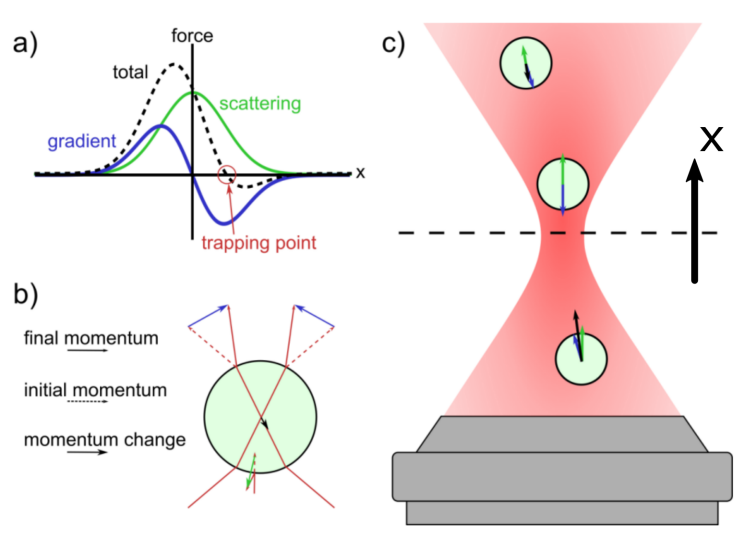

Figure 2.9: A) Two main force components near the focal point. B) Momentum vectors applied to a particle. C) Different forces and the overall force on a particle around the focus point of the laser. From [91] with modification. Copyright © University of Victoria

2.4.1 Experimental Setup for Optical Tweezers

An optical tweezer setup typically consists of a laser source to emit a continuous-wave, often with near-infrared wavelengths. It is used to provide sufficient trapping power without damaging heat sensitive samples.

An objective lens with a high numerical aperture (NA) is employed to tightly focus the laser beam, creating the necessary intensity gradient for trapping. Objectives with NA values greater than 1.0 are commonly used.

An inverted microscope is typically used for the observation of trapped particles and collect the signal. The sample is typically placed on a glass slide and positioned between the two microscope lenses using precision stages.

An avalanche photodiode (APD) is used to monitor the trapped particle by detecting changes in the transmitted laser light. The scattered light and vibrations of the particle can be measured with high accuracy.

2.4.2 Applications of Optical Tweezers

Optical tweezers can be used in many research fields including:

Biological Research

Optical tweezers have become significant tools in biological research. They are used to manipulate and study single molecules, such as DNA [92], RNA, and proteins [88], providing insights into their mechanical properties and interactions.

Cell Manipulation

In cellular biology, optical tweezers are used to trap and manipulate individual cells [93]. This enables the study of cell mechanics, cell interactions, and the effects of external forces on cellular processes.

Nanotechnology

In nanotechnology, optical tweezers are used to assemble and manipulate nanoparticles, nanowires, and other nanostructures. For instance, they can be used to fabricate nanowire networks and study their electrical properties [94].

Medical Diagnostics

Optical tweezers are employed in medical diagnostics to isolate and analyze individual cells or particles from biological samples [89]. This technique can be used to improve diagnostic accuracy and sensitivity.

2.4.3 Challenges for Using Optical Tweezers

Despite many advantages of optical tweezers, they have a few challenges. The most important challenge especially for bio-molecule applications is thermal damage. The intense laser light used in optical tweezers can cause thermal damage to biological samples. This limits their use in sensitive applications [80]. Minimizing this damage by using lower laser powers and optimizing trapping conditions can be helpful to mitigate this issue. Instrumentation complexity in traditional optical tweezer setups is another challenge. They require multiple microscope objective lenses and complex optical setups. It makes them less accessible for routine use. The proposed methods in this work will help in this regard.

2.4.4 Plasmonic Structures for Trapping

Plasmonic-assisted optical trapping uses the unique properties of plasmonic nanostructures to enhance the trapping efficiency of optical tweezers. By utilizing the strong electromagnetic fields generated at the surface of metallic nanostructures, the

trapping setup can confine particles to nanometer-scale regions, making it a powerful tool for manipulating nanoparticles and biological molecules. Localized surface plasmons have high intensities and improve the trapping stability.

The trapping efficiency of plasmonic-assisted optical tweezers is influenced by several factors, including the size and shape of the metallic nanostructures, the wavelength of the incident laser light, and the refractive index of the surrounding medium. By optimizing these parameters, we can achieve enhanced trapping forces and improved spatial resolution.

In an effort to reduce the loss and heat generation in the plasmonic resonators, aperture-assisted trapping has been used [80, 95]. In this approach, high intensity fields that are enough for trapping, are localized in small areas reducing the required laser power. Also the high intensity field areas are in contact with the rest of the metal layer and their generated heat will be transferred away from the trapping area. This will reduce the temperature of the trapping area and hence heat sensitive materials can be trapped. It allows the use of organic substances in the proximity of plasmonic resonators with the least amount of degradation. DNHs are a good example of these structures.

According to Bethe theory [40], transmission through an aperture is inversely proportional to the fourth power of light wavelength.

$$T \propto \frac{1}{\lambda^4} \tag{2.6}$$

If the refractive index of the material within the aperture changes, the wavelength of the light passing through it will also change, which in turn affects the transmission intensity [91].

$$\frac{T_2}{T_1} = (\frac{\lambda_1}{\lambda_2})^4 = (\frac{n_2}{n_1})^4 \tag{2.7}$$

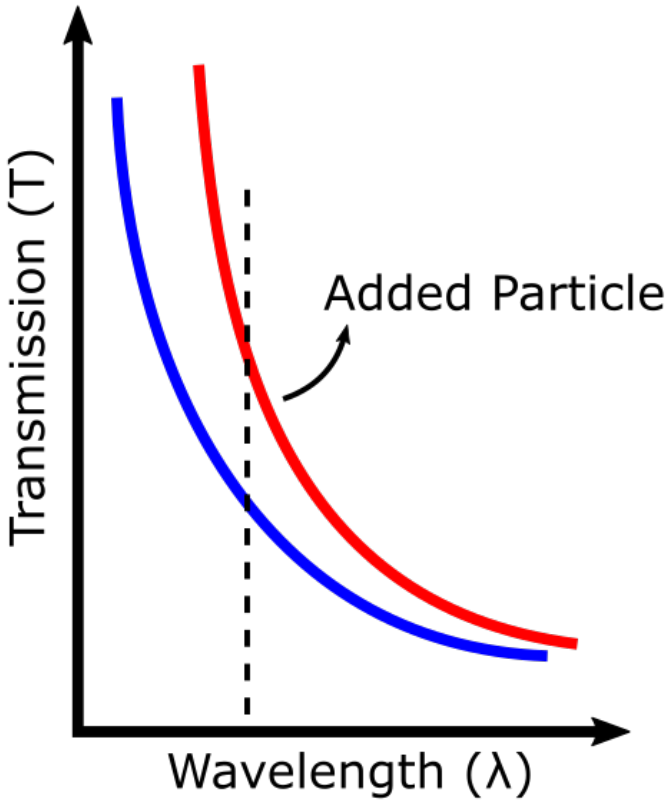

Figure 2.10: Adding a particle with a higher refractive index than the solution in the aperture, will increase the light transmission through the aperture.

Therefore, a small change in the refractive index can lead to a significant alteration in transmission. This modification can be achieved by introducing a nanoparticle into the aperture. This will be done by optical trapping and transmission measurement. The change in transmission can be seen in Figure 2.10.

To confine the electromagnetic waves in a sub-wavelength area, certain structures have been designed to enhance the field in an efficient way including DNH, bowtie aperture, circular nanohole array, c-shaped aperture and slit-groove aperture [96].

2.4.5 Summary of Past Works on Trapping in Double-Nanoholes

In recent years optical trapping using nanoholes created an opportunity to study nano-particles and single molecules. Having a strong field gradient over a small area on metal will create enough force to keep a nano-particle in place. This force pushes the particles from the area around and above the aperture towards the substrate where the aperture is formed. This force has minimal effect on the particle composition and does not need labeling for the particle. Thus, unlabeled particles can be characterized using this method.

Bio-molecules are mostly sensitive and can be damaged easily during many types of measurements. Some non-invasive measurements require high amounts of the particle in a solution and their detection sensitivity is low. On the other hand, optical trapping has the advantage of high sensitivity and requires less concentrations to be able to detect a particle in a solution.

The field enhancements in a DNH depend on wedge and gap plasmonic resonances [85]. The frequency of these resonances can be tuned by changing the dimensions of DNHs [97].

The tip separation in a DNH can determine the amount of transmission change in a trapping event. The field intensity and the amount of liquid between the tips will define the beam characteristics through the DNH. To maximize the increase in transmission when a particle is trapped, the tip separation should be a few nanometers bigger than the particle diameter. Figure 2.11 shows the transmission change when a 20 nm polystyrene bead is trapped for different tip separations. It shows that there is an optimum distance can be achieved by tuning the geometry of DNHs.

The movements of the particle trapped in a DNH, can be used to measure the stiffness of the trap. These Brownian movements can be monitored by measuring the transmission through the hole. Two common methods to analyze the transmission

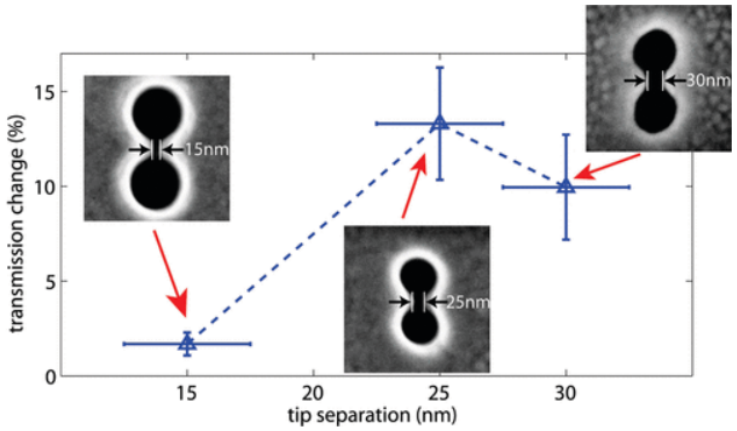

Figure 2.11: Transmission change for different tip separations in DNHs when a 20 nm polystyrene bead is trapped. Reprinted with permission from [98]. Copyright © 2011 American Chemical Society

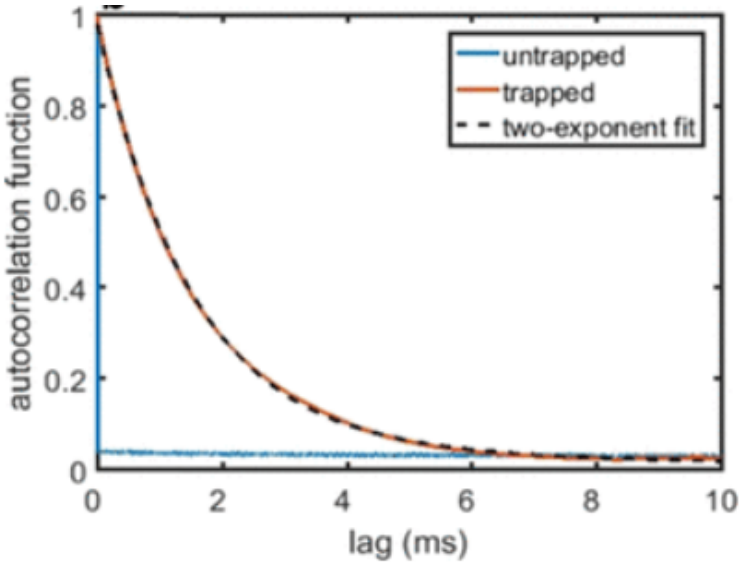

Figure 2.12: Autocorrelation function for trapping data of an egg white protein. Reprinted with permission from [88]. Copyright © 2018 American Chemical Society

data are autocorrelation [4] and power spectrum density [5]. These two measures are related by Fourier transform. Figure 2.12 shows the autocorrelation function for transmission data from trapping of an egg white protein. The curve for trapped state was fitted with a two exponent function.

Another way to determine how stable the trap is and how much force is needed to release the particle is to create a flow of liquid across the DNH. This had been investigated in a previous study [87] by measuring the flow rate required to release the particle. It was observed that by increasing the trapping laser power, more flow rate is required to get the particle out of the trap. Figure 2.13 shows the results of that experiment. It can be seen that by fitting a linear function to the data, the minimum power to keep the particle in trap with no flow can be determined and it agrees with experimental data.

By using the flow mechanism, it is possible to add different particles to the trapping location and see their interaction. In a study, bovine serum albumin (BSA) and anti-BSA were used to trap in a DNH and record the interaction data [79]. Another

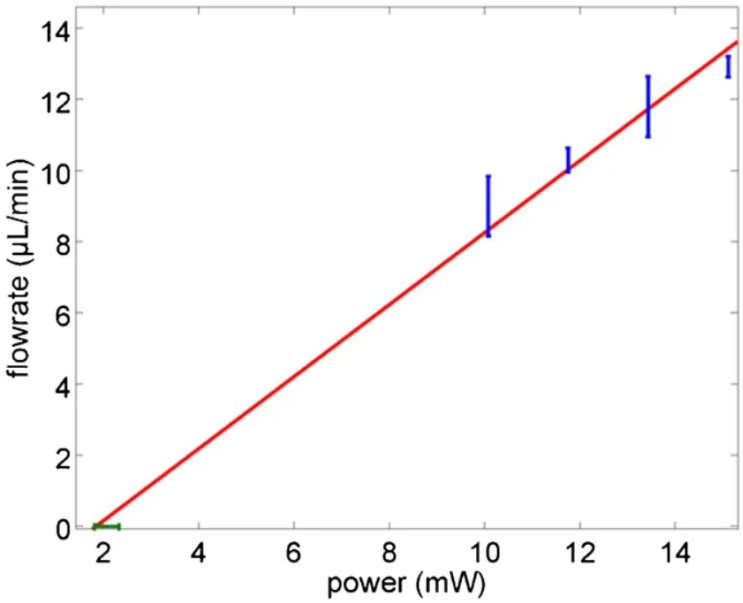

Figure 2.13: Critical flow rate for different incident laser powers for 20 nm polystyrene spheres. Reprinted with permission from [87]. Copyright © 2012 Springer Nature

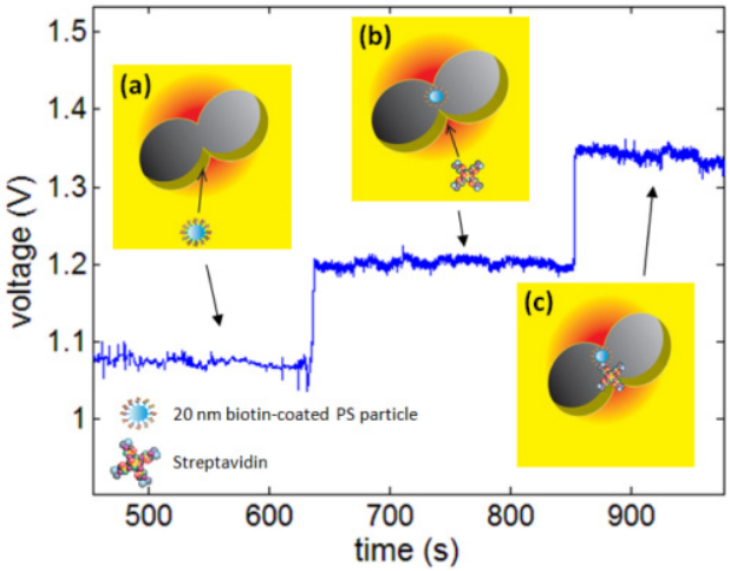

Figure 2.14: Trapping of biotin-coated polystyrene nano-particles and binding streptavidin to the trapped particle. From [49] Copyright © 2013 Optica Publishing Group

study used 20 nm biotin-coated polystyrene nano-particles and streptavidin [49]. The results are shown in figure 2.14. The binding of streptavidin to a trapped polystyrene particle changed the transmission signal which is different from the two particles trapping signal.

The folding and unfolding of BSA proteins have also been studied by changing the pH level of the flowing solution [99].

By using the transmission signal of a trapped particle, their size can be determined. Different weight and size determining methods have been used on proteins [78]. Other than sizing, Raman spectroscopy can be used to identify the trapped nano-particle [17, 100]. Figure 2.15 shows a Raman shift plot for a polystyrene nano-particle compared to a bulk polystyrene.

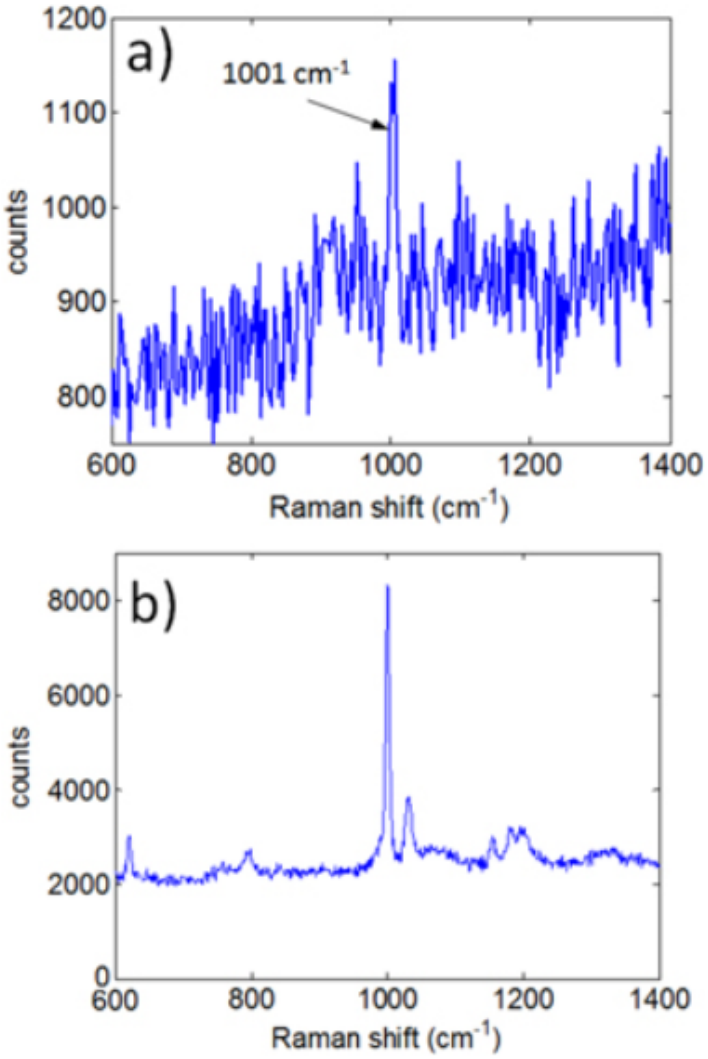

Figure 2.15: Raman spectrum of a) a trapped 20 nm polystyrene particle and b) bulk polystyrene particles. Single particle measurement is average of 5 spectra with an acquisition time of 5 minutes each, and the Savitzky-Golay filter is applied to the data. From [17] Copyright © 2015 IOP Publishing

2.5 Raman Spectroscopy

Raman spectroscopy is a method for the analysis of nanoparticles. It provides valuable information on molecular structures and their size variations [21–23, 101–106]. It can be used to study a single nanoparticle, for example, to explore their heterogeneity, finding trace materials or observing molecular reactions [105, 107–109]. Optical trapping can be used to isolate single nanoparticles. Optical trapping of single nanoparticles has been achieved using an intensely focused (NA = 1.25) Raman microscope objective and 120 mW of laser power, achieving 13 counts/second Raman signal for polystyrene beads with 40 nm diameter [110].

To achieve trapping for small particles and higher Raman signals, trapping with gap plasmons has been done in this work. Gap structures have been shown to be effective in enhancing Raman signal [111–122]. One approach to make gap plasmons around the particle is to trap metal nanoparticles. This will provide a gap enhancement between trapped metal nanoparticles [123–126]. Nanopores can also be used for trapping nanoparticles in solutions [92, 127, 128]. To perform Raman measurements of non-metallic particles, field enhancement from metallic aperture can be used. This enhancement has been achieved with rectangular and DNH apertures [17,100]. Previous works required top-down nanofabrication methods for the apertures and a custom optical tweezer setup to verify the trapping by measuring the transmission [17]. Overall, shaped nanoapertures have been widely used for trapping nanoparticles, including quantum dots and single proteins [44, 129–134].

There has been extensive research on single molecule and nanoparticle SERS measurements. Some examples are works on proteins [135], DNA [136, 137], extracellular vesicles [89], viruses [138], and other particles [139].

In this work, both custom and commercial optical trapping systems were used in reflection mode to observe the particle trapping on the Raman system with the

built-in camera. The camera is used both to identify DNHs for trapping and also observing the trapping event. To fabricate DNHs, a colloidal lithography method was used [84]. By using a commercial Raman system and bottom up fabrication method, this approach is highly accessible to a wide range of researchers. The DNHs enhance the trapping efficiency, and enhance the Raman signal, resulting in 400 counts/second with 14 mW of laser power for 21 nm diameter Titania nanoparticles.

2.5.1 Raman Shift Principles

Raman spectroscopy is a non-destructive analytical technique that provides detailed information about the molecular composition, structure, and interactions of a sample [140]. This technique is based on the inelastic scattering of light, usually from a laser, by the molecules in the sample. When the light hits the molecule, most of the scattered light is scattered elastically also known as Rayleigh scattering. In this case, the scattered light will have the same energy as the incident light. On the other hand, a small fraction of the light is inelastically scattered. It will result in a shift in the energy of the scattered photons by the amount of vibrational energy deposited or gained from the molecule. This type of scattering is known as the Raman scattering and the shift in energy is called Raman shift [91].

The Raman shift corresponds to the energy levels of the vibrations of the molecules in the sample or phonons. By measuring the frequency and intensity of the Raman scattered light, we can obtain a Raman spectrum that provides a unique fingerprint of the sample's molecular structure.

The Raman scattering mechanism can be explained by energy level transitions in a particle. When a photon from the laser interacts with a molecule, it can excite the electrons to a virtual energy state. The electron then relaxes back to a lower vibrational energy level, emitting a photon with a different energy than the incident

photon. This energy difference is the Raman shift and is the characteristic of the specific vibrational modes of the molecule.

The Raman shift is typically measured in wavenumbers (cm^{-1}) and is given by equation 2.8:

$$RamanShift(cm^{-1}) = \frac{10^7}{\lambda_{laser}} - \frac{10^7}{\lambda_{scattered}} \tag{2.8}$$

where λ_{laser} and $\lambda_{scattered}$ are in nm.

Raman scattering consists of two types of scattering:

- Stokes Scattering: This occurs when the scattered photon has lower energy than the incident photon, resulting in a positive Raman shift. It means that the scattered light has longer wavelength compared to the laser wavelength. Stokes scattering is the most common type observed in Raman spectroscopy.

- Anti-Stokes Scattering: This occurs when the scattered photon has a higher energy than the incident photon, resulting in a negative Raman shift. Anti-Stokes scattering is less common and typically weaker than Stokes scattering, because at ambient temperatures the population of molecules across vibrational states favor the vibrational ground state. Anti-Stokes Raman scattering requires the molecule to be in a vibrationally excited state.

Figure 2.16 shows the energy level transitions for Stokes and anti-Stokes scattering. It can be seen that Stokes scattering emits lower energy photons and has longer wavelength in the Raman shift spectrum.

2.5.2 Surface-Enhanced Raman Spectroscopy

Due to the weak nature of Raman signal intensity, having reliable measurements from small particles is challenging. Increasing the laser power can be helpful for enhancing

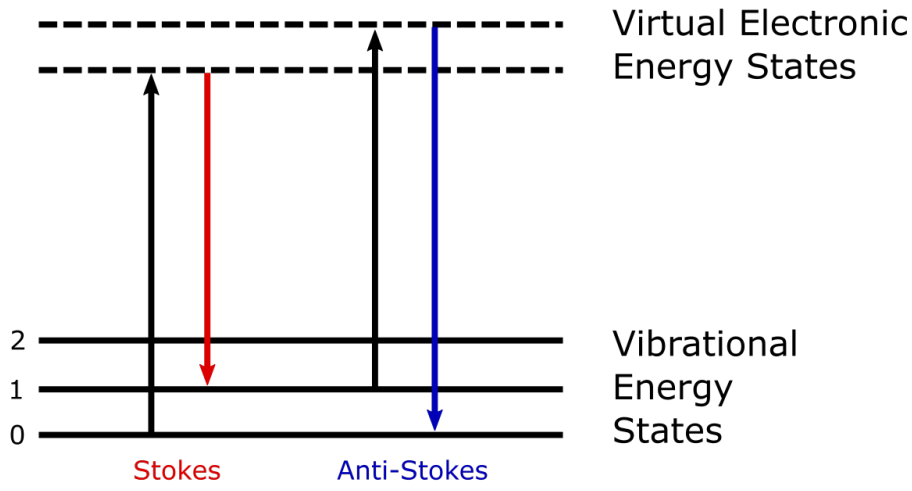

Figure 2.16: Stokes and anti-Stokes transitions. Black arrows are absorption. Red arrow is Stokes scattering and blue arrow is anti-Stokes scattering.

the Raman scattering but it has the potential to damage the sample. There are a few techniques that can overcome these challenges. In this work SERS has been studied and experiments were done using this method.

The fundamental principles of SERS can be broken down to these aspects:

Electromagnetic Enhancement

The primary mechanism behind SERS is the electromagnetic enhancement resulting from LSPRs [141, 142]. When light interacts with a patterned metal surface or nanostructure, it induces surface plasmons. These plasmons generate intense localized electromagnetic fields, particularly at the metal surface. Molecules near these surfaces experience high intensity electromagnetic fields. It increases the Raman scattered signal intensity.

Chemical Enhancement

A weaker mechanism, known as chemical enhancement, involves the interaction between the molecules stuck on the metal surface and the metal [142]. This interaction can result in charge transfer between the molecule and the metal. It changes the electronic state of the molecule and enhances the Raman scattering signal. This mechanism is weaker than the electromagnetic enhancement.

Substrate Design

The choice of substrate is critical in SERS. Commonly used substrates include nanostructured metals like gold, silver, and copper. These materials are chosen for their ability to support strong plasmon resonances in the visible and near-infrared regions of the spectrum. Substrate patterns such as nanoparticles, nanowires, and roughened metal surfaces can be optimized to maximize the enhancement effect [24].

These structured surfaces have regions of intense electromagnetic fields. They are typically located at the junctions of nanostructures [143] or sharp features on the metal surface [85]. These hot spots are responsible for the enhancement of the Raman signal and can enhance the detection sensitivity down to the single-molecule level [144].

The Raman shift observed in SERS, provides a fingerprint of the molecular vibrations and can be used to identify and characterize the molecules on the substrate. The enhancement provided by SERS allows for the detection of nanoparticles at low concentrations.

DNHs are used in this work as both the trapping medium and the SERS substrate for Raman enhancement. These apertures has multiple modes of LSPRs in their gap region which will provide extensive Raman enhancement.

2.5.3 Raman Enhancement in Double-Nanoholes

To calculate the Raman enhancement factor, we need the maximum electric field intensity relative to the laser intensity within the DNH. These fields are measured at both the laser wavelength and the scattering wavelength. The scattering wavelength is the wavelength that corresponds to one the peaks in the Raman spectrum. The Raman enhancement factor can be calculated [111] using equation 2.9

$$EF \propto \frac{|E_{local}(\omega_{ex})|^2}{|E_{laser}(\omega_{ex})|^2} \times \frac{|E_{local}(\omega_{scat})|^2}{|E_{laser}(\omega_{scat})|^2} \tag{2.9}$$

If the strongest peak is close to the laser wavelength, the excitation wavelength and scattering wavelength would be similar. It can be observed that the Raman signal is enhanced by approximately the fourth power of the field intensity, which itself is an enhancement compared to the laser field.

In a DNH, if the maximum field intensity is occurring in gap region, the field

intensity will increase by reducing the gap size.

Chapter 3

The New Approaches and Solutions

This chapter introduces a summary of the research work and contributions during my PhD program. First a new approach to optical trapping is proposed. This method will simplify and improve the current optical trapping systems that use nano-apertures. In this method, the trapping signal will be acquired by measuring the reflection beam from the aperture in the metal surface.

Next, an improved Raman spectroscopy method using a commercial Raman system is demonstrated. In this method, nano-apertures were used to trap nano-particles and amplify their Raman emission. It can be used as a SERS system to study nano-particle characteristics. The observation and verification of trapping is shown to be an effective approach to measure the aperture variation effects on the spectroscopy.

Next, a series of simulations on DNHs had been presented. The simulations were done on DNHs with different sizes to find the optimum size for a specific laser wavelength and how it reflects light. Also, the field enhancement profile and the maximum values for different frequencies have been determined. These simulations give valuable

insights about the required geometries for optimum trapping and Raman enhancements.

3.1 Reflection Mode Trapping

In a conventional optical trapping setup which works in transmission mode, the particle containing liquid will be placed between two objective lenses. One objective has a high magnification and will focus the laser beam on a small area on the sample. The other objective acts as a collector and will collimate the light to reach the detector. This transmitted light through the sample will be absorbed by a detector which is an avalanche photodiode (APD). In this method, most of the signal received by the APD is the transmission through the holes on the sample. If the aperture used for trapping is a DNH, the particle will be trapped in the gap region between the holes and will alter a portion of the transmitted light through the aperture. This transmitted laser beam can be used as the signal from the particle and the trapping event will be indicated by an increase in the APD output voltage and the increased amplitude of the voltage oscillations.

As seen in Figure 3.1 a conventional transmission trapping setup uses two objectives, the collector objective has a small numerical aperture and and low magnification, so it will collect a small portion of the focused beam. Due to the magnification mismatch between the two objectives, a big portion of the signal will be lost. If the collector objective was replaced by a high magnification one, the available space for the sample will be limited and not enough for proper placement of the liquid chamber.

On the other hand, if the reflected beam from the sample was collected and measured by one objective, most of the signal can be collected by that objective with a large numerical aperture and very small changes in the reflected light can be detected.

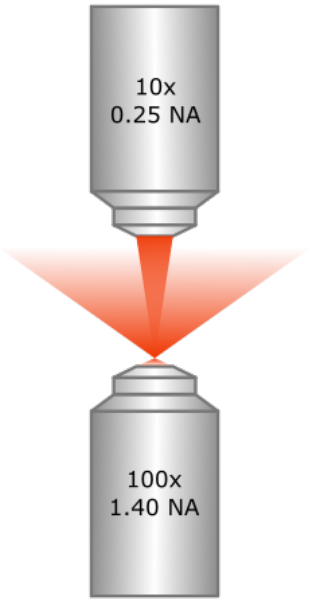

Figure 3.1: Laser beam focused between two objective lenses with overlapping focal points. The bottom objective focuses the laser beam and the top one collects the beam.

This small signal can be used to study the trapped particle.

The beam spot diameter can be found by equation 3.1 [145, 146]

$$D = 1.22\frac{\lambda}{NA} \tag{3.1}$$

in which, λ is the laser wavelength and NA is the numerical aperture of the microscope objective. By calculating the diameter of the beam spot on the sample, for different microscope objectives and laser wavelengths, we can determine suitable aperture sizes for the corresponding setup.

Figure 3.2 shows the Airy diameters compared to DNHs for two trapping setups with different objectives and laser wavelengths. It can be seen that minimizing the

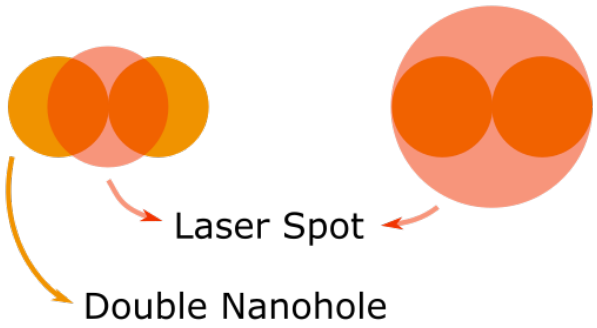

Figure 3.2: The beam spot on two DNHs for different setups. Hole diameters are 470 nm. The beam spot diameter on the left is 680 nm and on the right is 950 nm.

beam spot and maximizing the hole diameters, will cause the laser to only affect the gap separation on the DNH. Therefore, the reflection will result from the area in which the particle is trapped. This will eliminate the unwanted signal from the particle's surroundings.

The Airy diameter calculations for the two setups mentioned are shown in equations 3.2 and 3.3.

$$D_1 = 1.22 \times \frac{785\,nm}{1.4} = 684.1\,nm \tag{3.2}$$

$$D_2 = 1.22 \times \frac{980\,nm}{1.25} = 956.5\,nm \tag{3.3}$$

3.1.1 Sample Orientation

There are three methods to place a sample in an optical trapping setup. They are shown in Figure 3.3. The main difference between these methods is that the laser beam can either go through the liquid or through the glass to reach the gold layer. This will result in different plasmonic resonance frequencies that will form on the

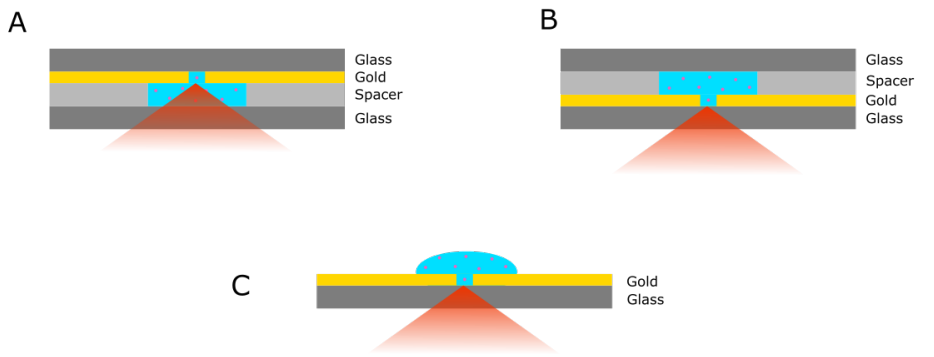

Figure 3.3: A) Laser beam in liquid. B) Laser beam on glass. C) Laser beam on glass with open chamber.

metal-dielectric interface because of the change in the dielectric layer. The dielectric layer is either water or glass. In this work, the glass was coated with Indium Tin oxide (ITO) before sputtering gold, to help with the adhesion of the gold and the glass. The ITO layer is very thin, transparent and conductive but its resistivity is higher than gold. Therefore, a significant portion of the plasmonic resonances will occur in the gold layer.

Most optical trapping setups use a closed chamber for keeping the liquid in place and the laser beam goes through the liquid to reach the aperture. If the sample is flipped, so that the liquid can be placed on top of the gold film, there is no need for a closed chamber as shown in Figure 3.3 (C). The simplicity of this method will allow the measurement of multiple sample solutions on one gold chip and it will accelerate the measurement process.

3.1.2 Optical Setup

In order to collect the trapping signal from the reflected beam off the apertures, a polarizing beam splitter was used. This beam splitter was placed in the laser path before the microscope objective. It was used to separate the two polarizations of

the reflected beam. The laser polarization was linear and able to pass through the beam splitter but the perpendicular linear polarization would be reflected towards another direction. This method can separate the orthogonal polarization from the laser polarization. The reflected beam with orthogonal polarization can then be collected and detected by an APD. The detected trapping signal can be used to determine the characteristics of the holes and particles.

A schematic of the reflection trapping setup is depicted in Figure 3.4 (C). The laser wavelength was 785 nm (z-laser Z80M18S3) and it was linearly polarized. It goes through a polarizing beam splitter (PBS). The beam splitter transmits the laser beam which has its polarization in the X direction. If the beam polarization is in the Y direction, it will be reflected. After the beam splitter, the input laser goes through a microscope objective lens (100 $\times$ 1.40 NA) to be focused on the sample. The power of the laser beam was measured before the objective lens and it was 10 mW. The DNH on the sample was at 45° compared to the laser linear polarization direction. Therefore, the reflected beam from the DNH has two orthogonal polarizations and it goes through the polarizing beam splitter. The polarization that is perpendicular to the laser polarization will be reflected by the beam splitter and goes into the measurement path to be detected by an APD.

Figure 3.5 shows the sample as seen on the CMOS camera. In order to see the DNHs on the sample, an infrared LED was placed behind the it and the infrared light is transmitted through the apertures on the gold film. The infrared wavelength was 940 nm and it was visible on the CMOS camera. A polarizer was in front of the LED to polarize its light in the perpendicular direction compared to the polarizing beam splitter. Therefore, only the converted polarization will reach the camera. This will highlight the location of the DNHs that have a 45° angle to the LED light polarization, as shown in Figure 3.5 (A). In Figure 3.5 (B) we can see all apertures without the

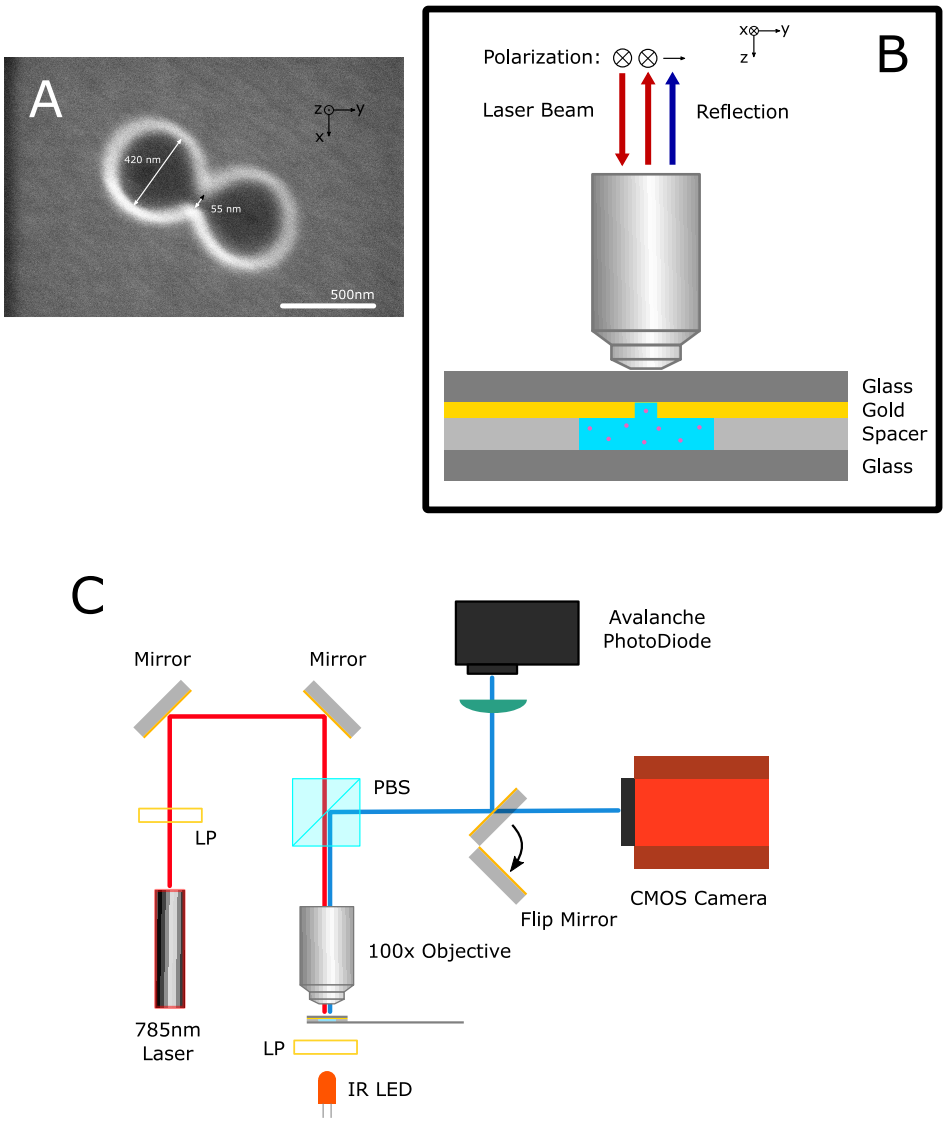

Figure 3.4: A) SEM image of a DNH on the gold film. Laser polarization is along X and reflected polarization is along Y axis. B) Sample structure. C) Schematic of the optical setup. LP: linear polarizer. PBS: polarizing beam splitter. From [28]

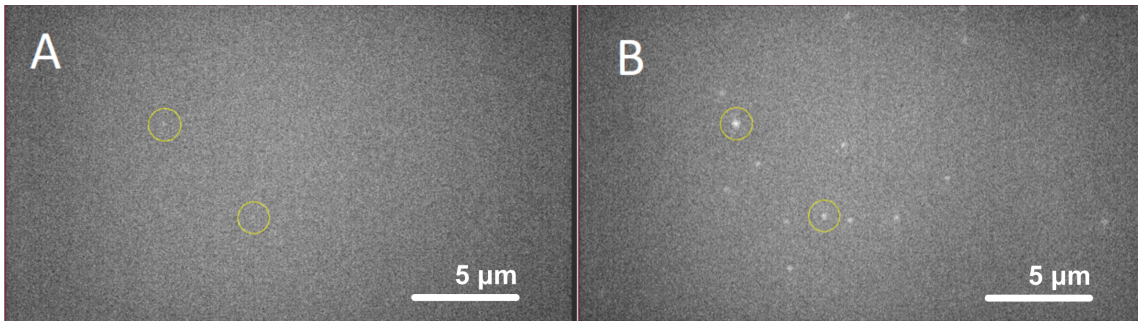

Figure 3.5: CMOS camera images. A) With polarizer in front of the LED. B) Without polarizer for LED. From [28] Copyright © 2023 Optica Publishing Group.

polarizer in front of the LED. If the solution is opaque, The LED can be placed before the beam splitter on the other side of the sample by using a dichroic mirror in the laser path and illuminate the sample with the same objective lens as the laser. Using this method will free up one side of the sample; but for simplicity and ease of polarization manipulation, it was placed behind the sample as seen in Figure 3.4 (C).

3.1.3 FDTD Simulations of Polarization Manipulation

To have a better understanding and determine the polarization-dependent reflection from tilted DNHs, simulations using Ansys Lumerical (FDTD) has been done. In these simulations, a structure similar to the experimental setup was used, and all possible orientations of laser polarization relative to the DNHs were simulated. The simulation results consisted of the electric field intensity around the DNHs and near the gold surface. The reflection and transmission intensities in the frequency domain were also monitored. After doing all simulations, degree of polarization was calculated using the simulation results. This parameter is used to determine the optimum value for the polarization orientations and to see how these orientations can affect the quality of trapping and resulting signals.

Simulations Setup

For the source, a 'total field scattered field' source was used with dimensions of 700 nm $\times$ 700 nm $\times$ 100 nm, encompassing the DNH and the 70 nm thick gold film. This source is used to simulate plane-wave excitation and avoid aperturing effects. In the experiments, a focused beam was used and it does not have a constant intensity on the focus plane, but in the simulations, the excitation wave was constant on the incident surface.

The mesh type used in the simulations was 'auto non-uniform'. This type of mesh will create elements with varying dimensions. The size of each element is smaller in areas with more complex geometries or higher refractive index contrasts. Thus, the simulation accuracy will remain high while the performance improves. Its accuracy was set to 5 and mesh refinement was set to 'staircase'.

For the gold material properties, data from Johnson and Christy [147] was used. For glass and water we used data from Palik [86]. The boundary conditions were set to "Perfectly Matched Layer" and its dimensions were 1.2 μm $\times$ 1.2 μm $\times$ 2 μm to ensure no wave reflection from the boundaries.

Two monitors were placed near the gold layer to measure the electrical field intensity, transmission and reflection of the incident wave. Figure 3.6 shows the reflection spectrum from the DNH in frequency domain. The electric field intensity around the DNH is shown in Figure 3.7. It can be seen that a high intensity electric field is formed in the gap and in the two holes. To measure a small change in the reflection beam that was caused by a trapped nanoparticle in the gap, we should selectively collect the cross polarized reflected light from the DNH.

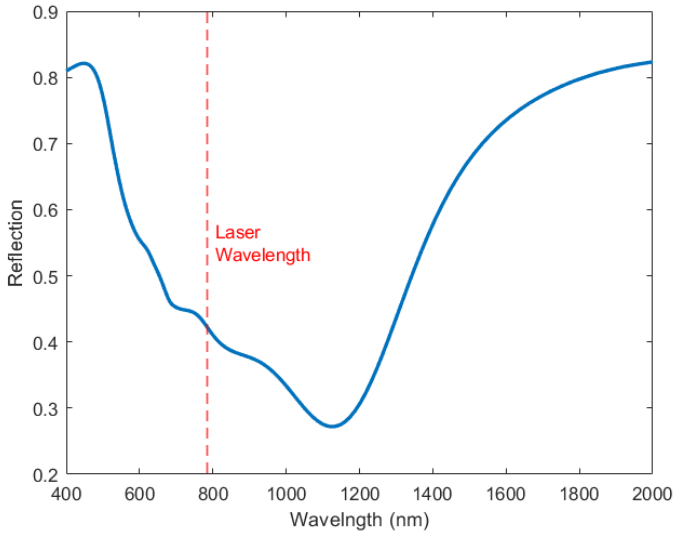

Figure 3.6: Simulated reflection spectrum of a DNH with the laser shown at 785 nm. The hole diameter is 420 nm and the gap size is 55 nm.

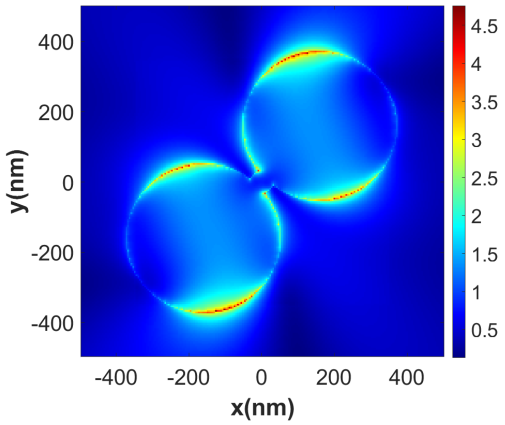

Figure 3.7: Electric field intensity around a DNH with the laser polarization along y axis. From [28] Copyright © 2023 Optica Publishing Group.

Degree of Polarization

To have a measure of how polarized the reflected light is, we can use degree of polarization. By calculating this parameter, we can see how much of the light changed polarization after reflecting from a DNH. To find this, a series of simulations had been done by varying the incident light polarization on a DNH. Then, the reflected light polarization was measured and it created a polarization ellipse shown in figure 3.8. It can be seen that most of the light is reflected with the same polarization that it had. A small portion of light will reflect at an orthogonal polarization.

To show the cross polarized scattering from a DNH, polarization ellipse for reflected light has been plotted using FDTD simulations. The polarization ellipse shown in figure 3.8 is for the reflected light from a DNH. The incident light has an S polarization and the long axis of the DNH is at 45° with respect to the incident light polarization.

To calculate the degree of polarization, the reflected light intensity was monitored and the intensity at two orthogonal polarizations was used as the maximum and the minimum intensity for the degree of polarization. The calculated degree of polarization for different polarization angles of the incident light from simulation results is shown in figure 3.9. Degree of polarization is defined in Eq. 3.4.

$$V = \frac{I_{\max} - I_{\min}}{I_{\max} + I_{\min}} \tag{3.4}$$

where $I_{\max}$ and $I_{\min}$ are the light intensities corresponding to the maximum and minimum polarizations, respectively. The maximum follows the incident laser polarization and minimum is the orthogonal reflection polarization.

To have a better representation of the DNH polarization manipulation capabilities, $1 - V$ was calculated and plotted in figure 3.9. It shows the plot for 1 minus degree

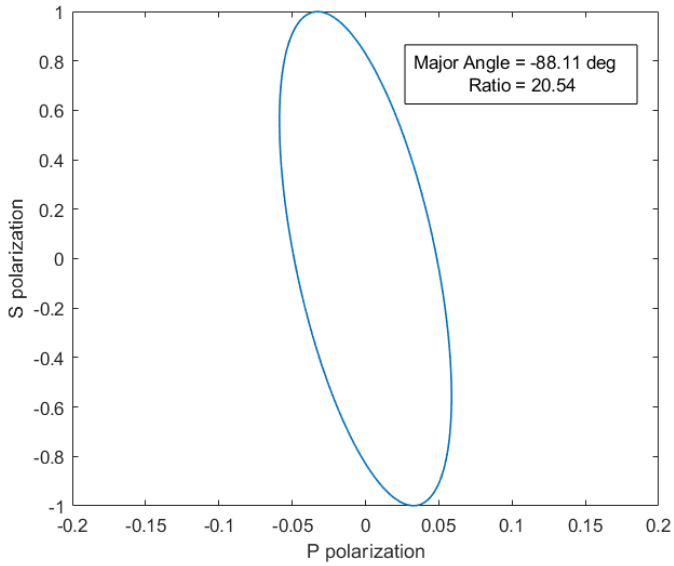

Figure 3.8: Simulated polarization ellipse for a DNH with an incident light with a polarization at 45° with respect to the long axis of the DNH.

of polarization for different polarization angles of the incident beam. The DNH orientation is constant in these simulations.

From Figure 3.9, we can see that 8.1% of the incident light is reflected with an orthogonal polarization compared to the incident polarization. This is the case when the incident beam polarization is at 45° with respect to the long axis of the DNH. $1-V$ values tell us how much the DNH will scatter the incident light into the orthogonal polarization.

3.2 Raman Spectroscopy of Nanoparticles

In this section, a new method for using a Raman system for nanoparticles is proposed. By utilizing DNHs, single nanoparticles can be trapped by the Raman system's laser and their spectrum can be measured at the same time. In this method, there is no need for two different lasers for trapping and spectroscopy. It can be used by any

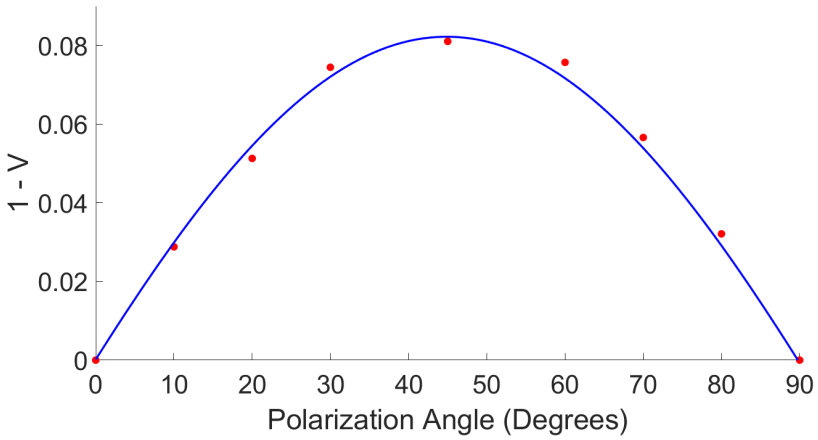

Figure 3.9: 1 minus the degree of polarization for different polarization angles of the laser light with respect to the long axis of the DNH from simulation results fitted with a sinusoidal function. From [28] Copyright © 2023 Optica Publishing Group.

conventional Raman system and there is no need for custom optical tweezer setups. The convenience of Raman spectroscopy combined with the capabilities of DNHs can be used to detect nano-scale particles in solutions with low concentrations.

Using DNHs in Raman spectroscopy has two main advantages. One is the optical trapping capability. Being able to trap a nanoparticle and isolate it from other substances, means that we can have a strong and precise Raman scattering collection. This will make the measurement more reliable and also make it possible to measure small particles that are not concentrated enough to be measured by conventional Raman spectroscopy.

The second advantage is the Raman enhancement. Many SERS methods have been in use to increase the intensity of Raman scattering. Some of these methods require a solution with high concentrations to cover the surface and make it possible to have an acceptable level of signal-to-noise ratio. But by using DNHs, the Raman laser will create a resonant surface plasmon around the aperture. This leads to a strong electric field on the gold surface around the holes. After trapping a particle in the aperture, it will be in proximity to the enhanced field, thereby amplifying its Raman scattering.

3.2.1 Double Nanohole Mapping

The colloidal lithography method used to fabrication DNHs, results in holes on the gold surface with different shapes. The holes can be single, double, or more clumped in some locations. The goal is to find DNHs on the sample. These DNHs are spread randomly on the sample and they have different orientations. In order to locate them and determine their orientation, scanning electron microscopy (SEM) can be used [148].

With careful fabrication to ensure a hole distribution that avoids clumping, it is

possible to use the camera image on the Raman system to differentiate double and single nanoholes on the sample. Also, the orientation of DNHs can be estimated with a high accuracy. On figure 3.10 SEM images and camera images are shown side by side to imply the method used to locate DNHs. It can be seen that double nanoles can be identified for trapping on the Raman system without the need to use SEM beforehand. In other words, finding DNHs does not require an SEM.

The camera image uses white light to illuminate the sample. The difference between double and single nanoholes can be seen in Figures 3.10(B) and (D). For confirmation, SEM images were taken after the measurements to show that the holes that were used were DNHs as shown in Figures 3.10(A) and (C). In the case that a hole was in fact two holes close to each other, the camera image cannot show that but the observation of weak Raman enhancement will show that it is not a DNH. This is another method to confirm the shape of the aperture.

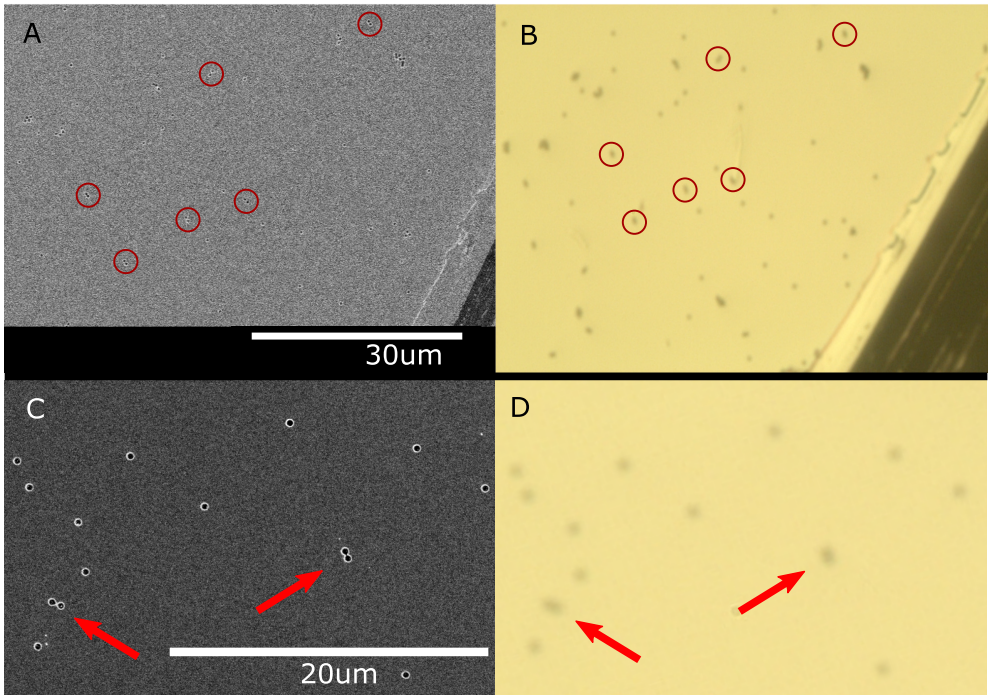

Figure 3.10: A) SEM image of the sample with DNHs circled. B) Camera image of the same area of the sample on the Raman system with the same DNHs circled. C) SEM image of single and DNHs. D) Camera image of single and DNHs. DNHs are indicated by arrows. Reprinted with permission from [29]. Copyright 2024 American Chemical Society.

Chapter 4

Experiments and Results

4.1 Sample Fabrication

The first step for aperture assisted optical trapping is to make the apertures. Apertures used in this work are double-nanoholes on gold. There are few methods to fabricate double-nanoholes [80]. Most of these methods are costly and require complicated procedures and expensive equipment. A widely available technique for aperture fabrication is to use colloidal lithography [66,149]. By drop-coating nano-spheres on a surface and expecting the desired pattern to form, we can have apertures with different orientations and shapes. Another benefit of this approach is that in one fabrication run, multiple apertures will be formed. Thus the chances of having hundreds of intended structures is possible. In this way, by going through one fabrication process, hundreds of different apertures will be created and can be used in multiple experiments with different requirements.

In this work, to make DNHs, a colloidal lithography method was used to create randomly distributed DNHs in a 70 nm thick gold film [148]. The fabrication starts by picking a glass slide with a 5 nm layer of indium tin oxide (ITO). Polystyrene

nanospheres with diameter of 800 nm in water and surfactant solution with 0.01% w/w concentration were drop coated on the ITO layer on the glass slides. In this process, the nanospheres will be randomly distributed on the surface and will form different orientations and structures. There will be a few single holes, double holes and more. By adjusting the concentration of the polystyrene solution, the probability of forming these apertures will change. The concentration used in this study created mostly single and DNHs. Knowing this we can use the camera on the optical setup to see the holes and by comparing the brightness of these apertures, singles and doubles can be differentiated.

After the drop coating step, nanosphere sizes should be modified to make the desired hole sizes. For this purpose, a plasma etching machine was used to reduce the size of the spheres. Using larger nanospheres and etching them to smaller diameters, creates smaller gap sizes compared to starting with smaller nanospheres. The polystyrene nanospheres on the ITO surface were placed in an oxygen plasma machine (Harrick, PDC-002) to be etched for 230 seconds at 30 W power to reduce their size. When the size of polystyrenes are decreased, the gap formed between double-nanoholes will also decrease. It is possible to make any hole size and gap size using this method, by changing the initial nanosphere size and the etching times [84].

After the etching step, the result will be nanospheres with smaller diameters than the original 800 nm. Therefore the resulting aperture size and cusp separation will be determined prior to sputtering the gold layer. The gold film was sputtered on the ITO layer with the nanospheres on it. The thickness of the gold film is 70 nm and it is measured by the quartz crystal microbalance (QCM) in the sputtering machine. After depositing the gold, the nanospheres should be removed to create holes in the gold film. For removing the nanospheres two methods can be used. The less destructive method is to use an adhesive tape to remove the beads [148] and the

aggressive but more effective method is to sonicate the sample in an ethanol bath for 2 to 5 minutes [84]. Both methods will successfully remove the beads to form nano apertures in the gold film. Both methods were used in this work. The resulting DNH is shown in Figure 3.4 (A) with hole diameter of 420 nm and cusp separation of 55 nm. This DNH and a few other sizes were used in the following experiments.

4.2 Reflection Mode Trapping

4.2.1 Solution Preparation

Three nanoparticle solutions were used in this work.

- Polystyrene particles with average diameter of 20 nm were in water with concentration of 0.02% w/v.
- Bovine Serum Albumin (BSA) was used with the concentration of 150 μM in phosphate buffered saline.
- Hexagonal boron nitride (hBN) nanoflakes were also trapped with average thickness of 3 to 4 layers and width of 50-100 nm with concentration of 5.4 μgmL^{-1} in a solution of water and ethanol [150].

These solutions were placed in a micro-well between the gold layer and a microscope cover slide. The laser comes through an aperture in the gold layer to reach the solution, traps a particle and reflects back. The laser was focused by an oil immersion 100$\times$ objective lens as shown in Figure 3.4 (B).

4.2.2 Trapping Experiments

When the focused laser traps a particle in the aperture, the reflection amplitude will increase. This reflection is from the gap region of the DNH because the polarizing

beam splitter separates this signal from the rest. The increase is caused by the shift in the LSP resonance frequency, which results from the addition of the particle in the gap. This value was measured by the APD and digitized by a Data Acquisition Device (Labjack U3-HV). This data was plotted in time domain to show the trapping event.

The trapping signals for polystyrene nanospheres and BSA can be seen in Figure 4.1. Figure 4.1 (A) shows a polystyrene particle already trapped, and then the laser beam had been blocked at 0.2 s to release the particle, followed by unblocking of the laser at 1 s. After about one second, a 1.84% change in the signal at 2 s indicates the trapping of the polystyrene nanosphere.

Figure 4.1 (B) shows blocking of the laser beam at 1 s to release the trapped BSA particle. Then by unblocking the laser at 1.8 s and waiting for about 1 s, the BSA particle was trapped again at 3.2 s and showed an increase in the voltage by 2.9%.

For trapping hBN nanoflakes, the setup was different and it used a 60× objective lens. Results are shown in figure 4.2. Figure 4.2 shows blocking of the laser beam at 1.2 s while an hBN nanoflake is trapped. This will release the particle. Then by unblocking the laser at 1.4 s and waiting for a while, an hBN nanoflake was trapped again at 2.2 s and it causes an increase in the signal by 4.8%.

It is possible to add an APD on the other side of the sample and collect the transmission signal. By measuring the transmitted light trough the DNH, we can compare it with the reflection signal in a trapping event. Figure 4.3 shows a trapping event for a 20 nm Polystyrene bead. To better show the trap data, a low-pass filter was applied to the data to reduce the visible noise. It can be seen that the transmission data has high amplitude noise that can cover the trapping signal and make it unnoticeable, unless a low-pass filter is applied to the data to see the signal properly. On the other hand, the reflection signal is more clear and has better signal-to-noise ratio for future

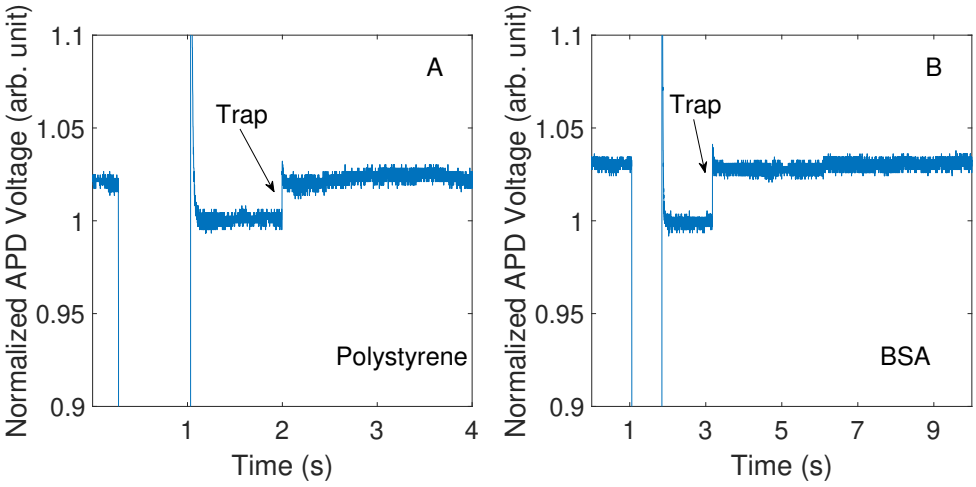

Figure 4.1: Normalized APD voltage while trapping A) Polystyrene nanoparticles and B) BSA. From [28] Copyright © 2023 Optica Publishing Group.

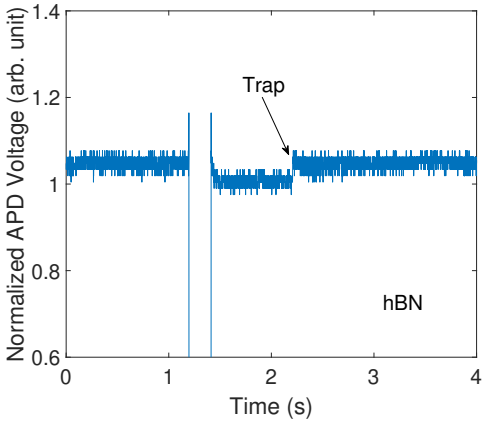

Figure 4.2: Normalized APD voltage while trapping hBN nanoflakes. From [28] Copyright © 2023 Optica Publishing Group.

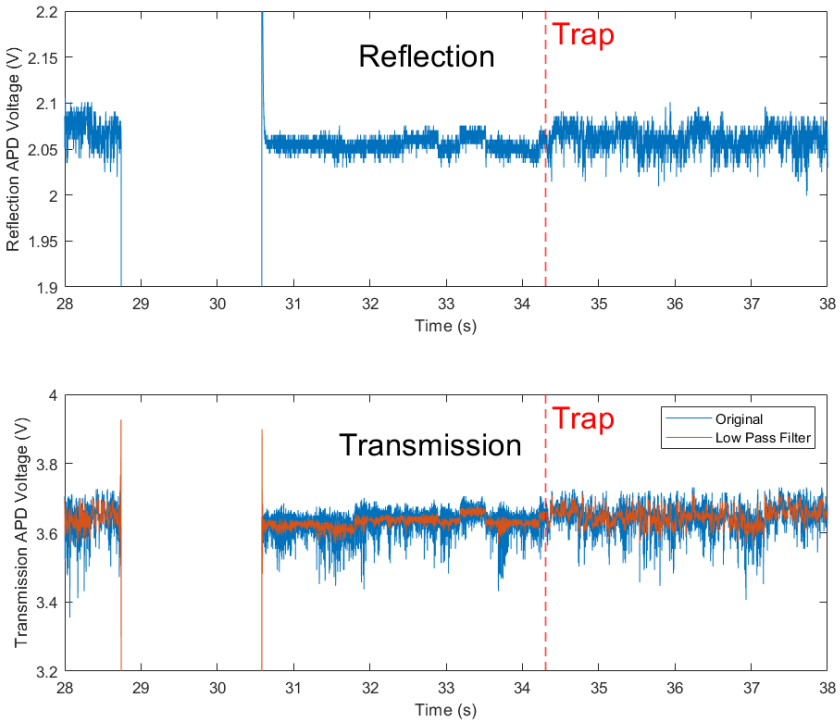

Figure 4.3: Trapping event of a 20 nm Polystyrene bead in reflection and transmission.

analysis.

Figure 4.3 shows that the signal amplitude is not changed considerably after trapping, but the noise amplitude has increased. The trapping event can be detected by observing the noise amplitude. The measured reflection signal is from the orthogonal part of the reflected beam and has a small increase in intensity after trapping similar to the transmission signal.

4.2.3 Raman Spectroscopy of Polystyrene Nanosphere

By using the reflection setup, it is easier to implement Raman measurements. To do Raman spectroscopy, a Raman probe was used to separate the laser beam and the Raman signal. A dichroic mirror inside the Raman probe with cut-off frequency near

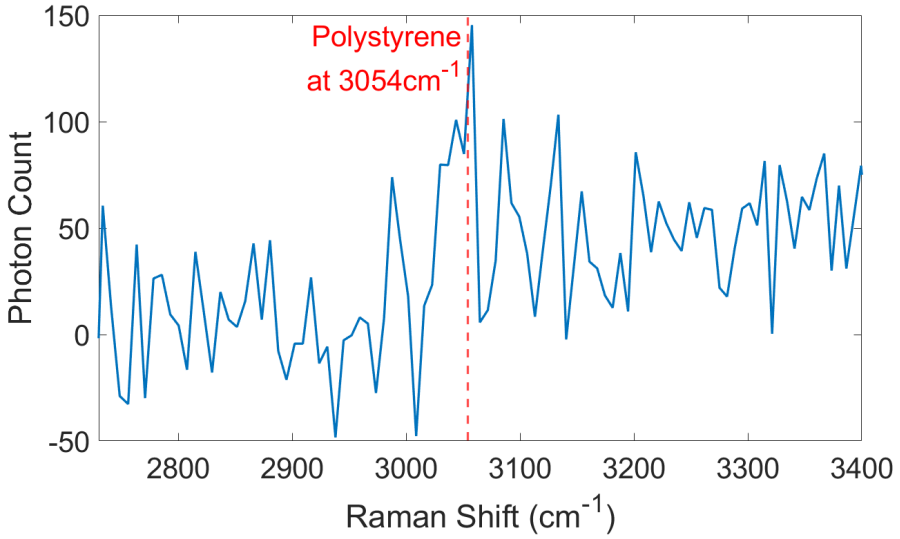

Figure 4.4: Raman spectra for a 20 nm polystyrene nanosphere showing the peak at 3054 cm^{-1}. From [28] Copyright © 2023 Optica Publishing Group.

785 nm will direct the excitation laser to a fiber and the light with longer wavelength to another fiber. In this way, one fiber will have the Stokes shift data. Connecting this fiber to a spectrometer will show the Raman signal.

The data is shown here for the reflection setup detected with the spectrometer (Ocean Optics QE65000). Improvements in the setup are required to obtain convincing results. Figure 4.4 shows the Raman shift spectrum for a 20 nm polystyrene nanosphere. The spectrometer integration time for this measurement was 3 minutes. This long integration times require the particle to remain in the trap. Due to the small size of the nanosphere and the weak Raman intensity of Polystyrene, a weak Raman peak is expected.

To have a useful signal to noise ratio, the integration time was 3 minutes. This will cause the spectrum to get saturated near the laser wavelength. This saturation will inhibit the ability to measure smaller Stokes shifts. Polystyrene has Raman peaks at different wavelengths and the most intense one is at 852 nm which corresponds to a Raman shift of 1001 cm^{-1} [17]. By using long integration times, this peak will fall

into the saturated part of the spectrum. To mitigate this issue, it is possible to look for peaks that are further away from the laser wavelength. The next Raman peak for polystyrene is at 3054 cm^{-1} which is far enough from the laser wavelength that we can increase the integration time to a few minutes. The intensity of this peak is lower than the main peak and in order to detect it, more accuracy in measurement and longer integration times are required. Because this peak is not close to the laser wavelength of 785 nm, the saturation of the spectrometer around laser peak will not affect the measurement.

4.3 Raman Spectroscopy of Nano-particles

4.3.1 Sample Fabrication

In the Raman experiments DNHs were used and were made using the same top-down method used before. Polystyrene nanospheres were used to create DNHs in the gold layer with desired gap sizes [84]. First, a solution of 600 nm polystyrene nanospheres from Alpha Nanotech with concentration of 0.3% w/v was prepared and drop coated on a no. 1 glass slide.

To reduce the holes and gaps dimensions, plasma etching was used on polystyrene beads. The duration of plasma etching was tuned to make the gaps formed by the touching nanospheres from 150 nm to 20 nm. The plasma etching reduces the diameter of the spheres so that they will be from 600 nm to 400 nm. These sizes were fabricated on different glass slides to be used in multiple measurements. Similar fabrications were done with different nanosphere sizes in previous works [84].

The resulting sizes for holes and gaps were observed experimentally. Calibration curves are required to have the parameters to precisely determine the hole sizes. For nano-hole fabrication, calibration curves are essential for ensuring that the dimensions

and properties of the fabricated holes meet the specified tolerances. Accurate calibration allows for the detection of any deviations in the fabrication process, enabling adjustments to be made to maintain high-quality standards.

The plasma etching machine used in this work was Harrick PDC-002. Polystyrene sizes were reduced in the etching process to create precise gap sizes between 20 nm and 60 nm [28]. In the process, the resulted nano-holes had a diameter of approximately 400 nm. After preparing the spheres with the desired sizes, the glass slides were coated with 100 nm of gold in a Mantis sputtering machine. Mantis sputtering machine has a quartz crystal microbalance (QCM) to measure the thickness of the sputtered gold. After depositing the gold, polystyrene beads were removed by sonication in ethanol. This makes the holes appear in the gold film.

The distribution of double nano-holes on the gold film depends on the concentration of polystyrene nanospheres in the solution. The optimum concentration will only create single holes and DNHs with no clusters of more than two holes. This will make is easier to identify DNHs on the camera on the setup. On the camera, DNHs are brighter and can be differentiated from single holes. By having more than two holes adjacent to each other on the sample other holes will be mistaken for DNHs [148].

The particles used is the experiment for Raman spectroscopy was Titania (TiO_2). A titania powder from Sigma-Aldrich (718467) with particle sizes of 21 nm was diluted in water. This solution was dropped on a microwell on the gold film and covered by a cover slip. The microwell was formed by stickers from Grace Bio-Labs SecureSeal with thickness of 0.12 mm. The cover slip thickness was No. 1 (130 - 160 μm thick). After sealing the titania solution on the sample, it was transferred to the Renishaw InVia Raman system. The cover slip was facing the 50$\times$ 0.75 NA objective to expose the solution to the Raman laser. Figure 4.5 shows the diagram and picture of the sample under the objective and a double nano-hole on the gold.

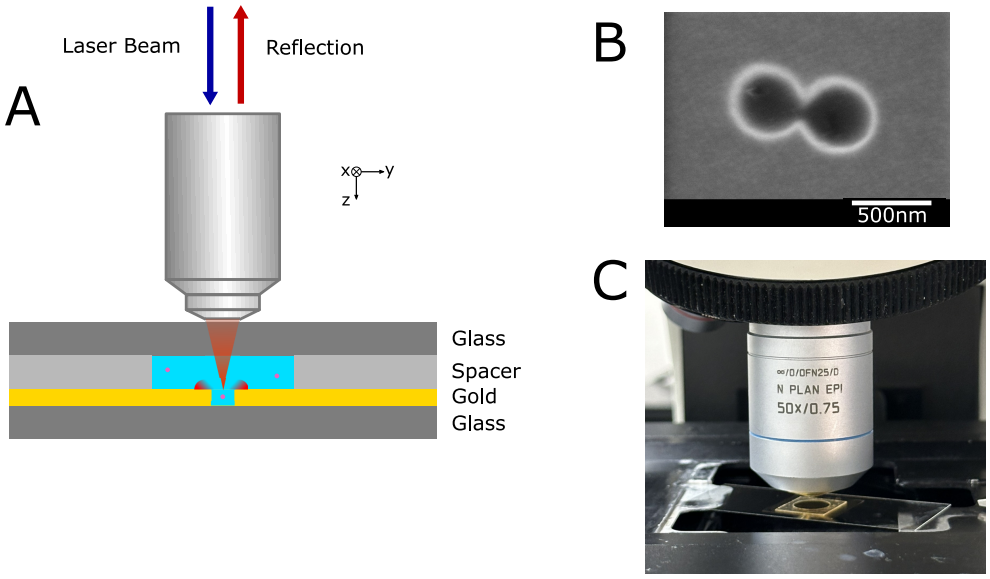

Figure 4.5: A) The gold sample with DNH and TiO_2 solution under Raman microscope objective. B) Scanning electron microscope image of a DNH in the gold layer. C) Picture of the sample under the microscope objective of the Raman system. Reprinted with permission from [29]. Copyright 2024 American Chemical Society.

The trapping laser was the same as the Raman excitation laser. Its wavelength was 785 nm and the signal for trapping and Raman scattering were measured in the reflection from the sample. The Raman system had a long pass filter to prevent the reflected laser beam from reaching the detector.

4.3.2 Camera Image Analysis

After finding a DNH on the sample using the camera on the Raman system, the laser will be turned on and focused properly on the aperture. After a few minutes a particle will be attracted to the trapping region and eventually be trapped in the DNH. This trapping event can be observed on the camera by visible changes in the laser fringes. This video can be recorded and analyzed [151].

An analysis of a trapping event is shown on figure 4.6. It shows a trapping event on the Renishaw InVia Raman system. The camera is receiving the reflection from the sample, so it sees a decrease in laser intensity. In conventional optical trapping setups with a detector in the transmission path, the intensity of the signal will increase when a particle in trapped in a DNH. To quantify the video data, a method similar to a previous work [151] was implimented. A line of pixels through the center of the beam spot in the video is chosen and its intensity is plotted over time in the shape of a waveform. A distinct change in the signal can be seen at 93 seconds. If we track only one pixel, for example pixel 794 of the line, it gives a typical optical trapping signal in a DNH.

This camera field of view is 90 μm by 58 μm and its resolution is 750 by 480 pixels. The video was recorded with 15 frames per second. Each pixel corresponds to a square with dimensions of 120 nm by 120 nm. Before the analysis, the video was converted to mpeg and the resolution becomes 1280 by 720 and the analysis was done on this file.

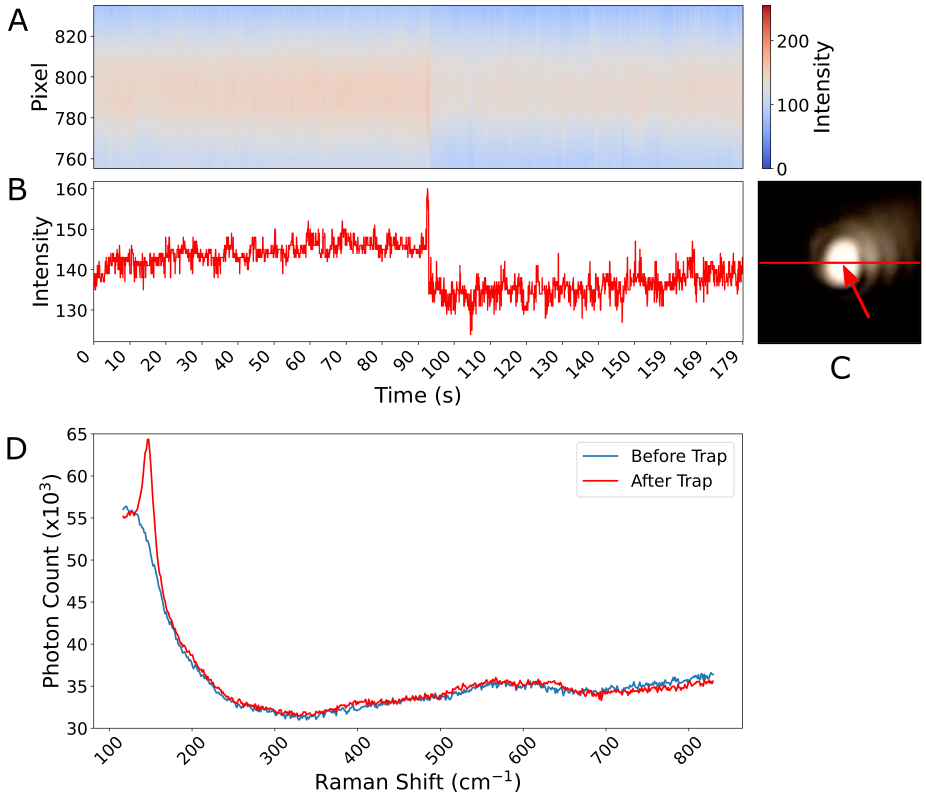

Figure 4.6: Trapping signal of Titania nanoparticle shown as a 2D waveform and 1D signal of pixel intensities over time. A line of pixels through the center of the beam spot is tracked over time. A) The change in camera image while trapping and monitoring along the red line. B) The change in camera image while trapping and monitoring a single pixel. C) Camera image showing the laser on the sample. D) Change in Raman spectrum showing Raman features after trapping. Reprinted with permission from [29]. Copyright 2024 American Chemical Society.

4.3.3 Raman Signal Measurements

After trapping Titania nanoparticle on a DNH, the Stokes shifts will appear on the spectrum. By comparing this data by the spectrum before the trap, Raman scattering signal fro Titania can be observed.

An example of a trapped TiO_2 Raman spectrum can be seen in figure 4.7. There are four strong peaks in the TiO_2 Raman spectrum and they are visible in this figure. The Stokes shift lines correspond to the molecular vibrations of anatase Titania, as reported here [152]. They correspond to these molecular vibrations: $E_{g(\nu 1)}$, $B_{1g(\nu 2)}$, $B_{1g(\nu 4)}$, $E_{g(\nu 6)}$. The integration time was 30 seconds for this measurement.

To determine how DNH sizes affect the Raman intensity, the intensity of the Raman spectrum at 145 cm^{-1} had been recorded for multiple samples with different aperture sizes. The intensity of this peak which is the highest one in Titania spectrum, for different DNHs with different cusp separations (gaps) are shown in Figure 4.8. As shown in this figure, by decreasing the gap size in the DNH, the Raman signal intensity will increase. This corresponds to a higher field intensity in the gap region due to the small cusp separation. It can be seen that decreasing the gap size increases the Raman intensity, and this is due to the plasmonic enhancement.

The values for Raman shifts like 145 cm^{-1} are based on a past work [153]. In the experiments, the shifts were shifted by 2 cm^{-1} compared to previous studies. The Raman system had that error for the calibration silicon as well and the data here were shifted accordingly to fix this issue.

As seen in the spectrum plot, the small peaks are visible at the expected locations, but their signal to noise ratio (SNR) was not enough to quantify the Raman enhancement. To improve these peaks, the integration time could be increased beyond the 30 seconds we used, but it would saturate the detector by the low wavenumber peak.

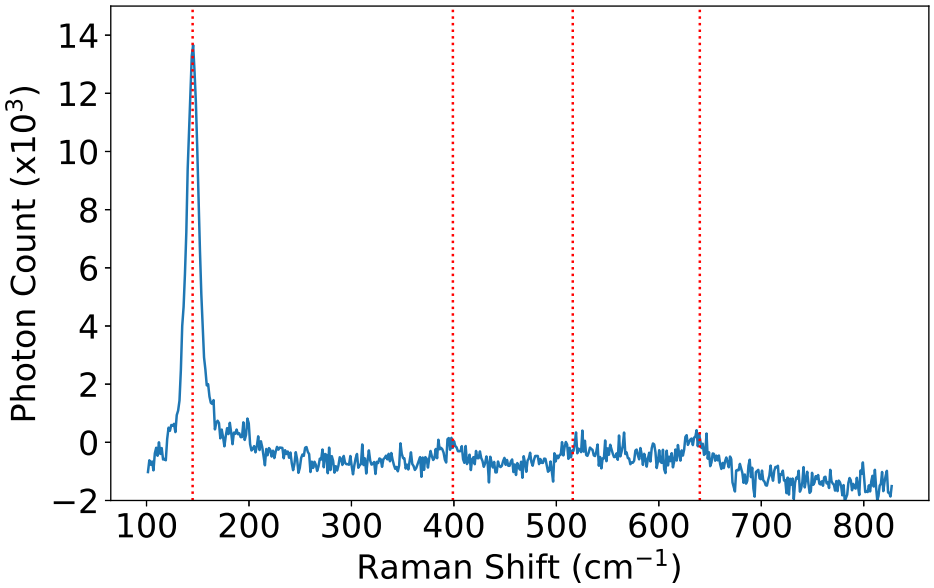

Figure 4.7: The Raman spectrum for a trapped TiO_2 particle showing peaks at 145 cm^{-1}, 399 cm^{-1}, 516 cm^{-1} and 640 cm^{-1} [153]. This spectrum is obtained by subtracting the Raman signals measured before and after trapping shown in figure 4.6 (D). Reprinted with permission from [29]. Copyright 2024 American Chemical Society.

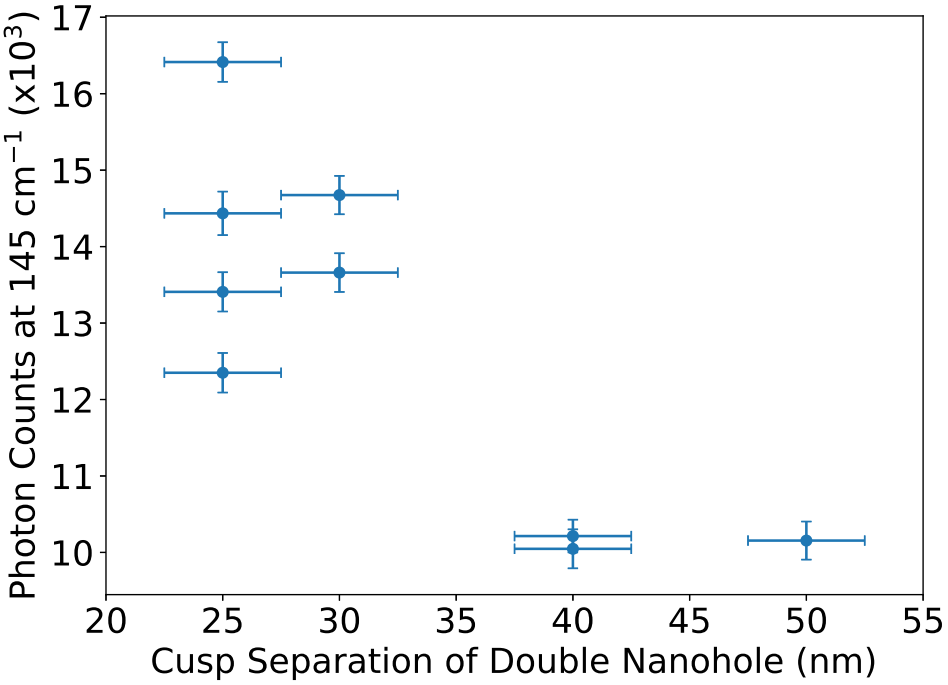

Figure 4.8: The intensity of Raman signal at 145 cm^{-1} for TiO_2 at different gap sizes of DNHs. Vertical error bars are from the shot noise and horizontal error bars are from the size measurement at SEM. Reprinted with permission from [29]. Copyright 2024 American Chemical Society.

Chapter 5

Evaluation, Analysis and Comparisons

5.1 Reflection Mode Trapping

The use of polarization symmetry breaking in the context of reflection-mode trapping is an innovative in this field. We demonstrated that this technique enhances the trapping forces, which is significant in its form. By tilting the DNHs and break the symmetry, the effectiveness of trapping event increases. This opens up new possibilities for more precise and efficient manipulation of nanoparticles, which can have significant implications in fields like biophysics and nanotechnology.

The experimental results were collected precisely and they showed enhancement and practicality in trapping particles compared to traditional methods. The experimental data, supported by robust theoretical models, demonstrate a marked improvement in trapping efficiency compared to traditional methods. The use of polarization symmetry breaking is a distinctive and creative approach, setting this research apart in the field of optical trapping.

Some limitations of this approach should be noted. The specialized nature of the experimental setup could pose challenges for replication by other researchers without similar equipment.

The results of this study are promising and highlight a novel approach to optical trapping. The combination of theoretical and experimental work sets a solid foundation for future research. This technique can be adapted and integrated into practical applications, and further advancements can be made.

5.2 Raman Spectroscopy

The approach presented here for Raman spectroscopy provides an accessible platform for the investigation of single nanoparticles in solutions. The main features that make this approach more accessible compared to other works are the use of a colloidal nanofabrication method which does not require a top-down lithography. Also, it is possible to identify DNHs and their orientations using the Raman system built in camera. Moreover, we can observe the trapping event by through the camera in reflection mode. Therefore, this approach is more accessible to researchers with access to a commercial Raman system.

Additionally, this method provides enhanced Raman signal from the DNH gap region, resulting in 400 counts/second with 14 mW of laser power and a 50× objective lens for measuring 21 nm particles. These results can be compared to a past work that obtained similar Raman signal intensities for Titania particles with a million times larger volume and without using metal nano-apertures [27]. Other parameters like laser wavelength, power and integration time were similar. Therefore, we show that the DNH apertures provide Raman enhancements that benefit both trapping and Raman signal for assessing the Raman spectra from individual nanoparticles.

It is possible to reuse the samples with DNHs at least ten times before they become contaminated and damaged. In order to reuse the samples, they were placed in acetone overnight, washed with ethanol and dried with dry nitrogen gas.

To optimize the DNH samples for improved Raman enhancement we can tune the size of the apertures and the gaps. In this work the focus was on 400 nm aperture diameters and cusp sizes approximately the size of the nanoparticle that we wanted to study. We also attempted using 200 nm apertures and they showed slightly higher Raman enhancement but not reported here.

Using cross-polarized detection with DNHs for the Raman signal is possible. This is impacted by the orientation of the DNH and their effect on polarization. If the DNH is at 45 degrees compared to the laser polarization, cross polarization can be used to minimize the elastic reflection of the incident laser [28].

It would be interesting to use this method to study heterogeneity of nanoparticles, for example, biological nanoparticles [99] or different crystal structures of nanoparticles.

Chapter 6

Conclusions

Nanostructures including DNH have been extensively used in optical trapping applications. These apertures are capable of isolating and characterizing single molecules and are able to give insight over the mechanics of nanoparticles. Investigating biomolecules have been a challenge in single molecule levels because of their sensitivity to small modifications. But utilizing optical tweezers created the opportunity to isolate and manipulate a single molecule.

Single particle manipulation and analysis is a powerful technique. It holds significant potential for advancing research across various scientific disciplines by enabling the precise examination and control of individual particles. This method allows researchers to gain deeper insights into the behaviors and properties of isolated molecules. This can be particularly valuable in fields such as quantum technology, biochemistry, and medicine, where understanding the interactions and dynamics at the molecular level is crucial. The ability to manipulate single particles opens up new possibilities for studying complex biological processes, developing new medication, and improving the design of nanoparticles. As a result, single particle manipulation and analysis is set to become a crucial tool for future scientific discoveries and

innovations.

6.1 Reflection Mode Trapping

The reflection geometry enables a simpler optical setup compared to traditional systems. Because there is no need to have two collinear objectives on both sides of the sample. The reflection setup uses the same objective for excitation and collection of plasmonic resonances. This method will free up space on one side of the sample. It will allow the manipulation of the sample and solution. For example it can be used to add opaque solutions and microfluidics to the trapping site on the chip. Using only one objective can reduce the cost of the trapping setup and simplify its maintenance.

There are numerous past works that have used reflection to monitor the trapped particle, but they did not exploit the polarization effects of the nanoaperture to isolate the reflected signal from the trapping area [154]. By using the polarization separation of the reflected light, it is possible to achieve an improved signal to noise ratio and more stable trapping.

With the utilization of the reflection measurement and its unique sample placement, we can work with highly scattering or opaque samples. Because these types of solutions do not transmit light efficiently, a conventional trapping setup is not able to show the trapping event on the sample. A few examples of these solutions include measuring asphaltene properties from crude oil [155] and blood serum analysis [156].

Addition of microfluidics equipment to the setup will be easier when we have more free space on one side of the sample, because there will be more space for connecting tubing and flow structures [87]. Several previous works have shown the benefits of combining DNHs with nanopores [157, 158] and those approaches can benefit from the proposed reflection geometry.

In future works on this subject, with the aim of improving the Raman spectroscopy, the poor quality fiber-probe Raman filter can be replaced by a free-space short-pass or notch filter to block the laser light. Better Raman signals had been achieved in similar setups in the past [17, 100]. With this method and improvements, we expect to measure a stronger reflected Raman signal, which will help us identify the trapped nanoparticle. This can be a major break-through in identifying nanoparticles such as proteins and antibodies.

6.2 Raman Spectroscopy

This dissertation demonstrates the use of DNH with a bottom-up fabrication process for optical trapping and Raman spectroscopy of single nanoparticles on a commercial Raman microscopy system in reflection mode. The ability to use these DNH for Raman spectroscopy makes this approach accessible to a wide range of researchers. Top-down nanofabrication or custom laser tweezer systems are not available to many researchers.

The ability to locate the apertures, their orientation and detecting a trapped particle using the camera integrated in the Raman microscope system had been demonstrated in this work. Based on these capabilities, it is believed that it will be an attractive approach to analyze heterogeneity in nanoparticles. Some examples of this analysis method are analyzing differences in crystal structure of solids or biological properties of bio-molecules.

For extending this method by future researchers, it is possible to use the laser to increase the sample temperature and possibly observe conformational changes in the molecules or interactions between them in real time. Recent research on these applications implies that aperture trapping can be effective in studying various particles

and the temperature dependence of their characteristics. [129, 137, 159–163].

Bibliography

[1] Elba Mauriz and Laura M Lechuga. Plasmonic biosensors for single-molecule biomedical analysis. *Biosensors*, 11(4):123, 2021.

[2] Yong-Ho Kim, Dongho Park, Jungho Hwang, and Yong-Jun Kim. Integrated particle detection chip for environmental monitoring. *Lab on a Chip*, 8(11):1950–1956, 2008.

[3] Zhao Yue, Fred Lisdat, Wolfgang J Parak, Stephen G Hickey, Liping Tu, Nadeem Sabir, Dirk Dorfs, and Nadja C Bigall. Quantum-dot-based photoelectrochemical sensors for chemical and biological detection. *ACS Applied Materials & Interfaces*, 5(8):2800–2814, 2013.

[4] Abhay Kotnala and Reuven Gordon. Quantification of high-efficiency trapping of nanoparticles in a double nanohole optical tweezer. *Nano Letters*, 14(2):853–856, 2014.

[5] Yi Deng, John Bechhoefer, and Nancy R Forde. Brownian motion in a modulated optical trap. *Journal of Optics A: Pure and Applied Optics*, 9(8):S256, 2007.

[6] L Andrew Lyon, Christine D Keating, Audrey P Fox, Bonnie E Baker, Lin He, Sheila R Nicewarner, Shawn P Mulvaney, and Michael J Natan. Raman spectroscopy. *Analytical Chemistry*, 70(12):341–362, 1998.

[7] Katrin Kneipp, Harald Kneipp, Irving Itzkan, Ramachandra R Dasari, and Michael S Feld. Ultrasensitive chemical analysis by raman spectroscopy. *Chemical Reviews*, 99(10):2957–2976, 1999.

[8] Andrés Cantarero. Raman scattering applied to materials science. *Procedia Materials Science*, 9:113–122, 2015.

[9] Giuseppe Pezzotti. Raman spectroscopy in cell biology and microbiology. *Journal of Raman Spectroscopy*, 52(12):2348–2443, 2021.

[10] L-P Choo-Smith, Howell GM Edwards, Hubert Ph Endtz, Johan M Kros, Freerk Heule, Hugh Barr, Joe Sam Robinson Jr, Hajo A Bruining, and Gerwin J Puppels. Medical applications of raman spectroscopy: from proof of principle to clinical implementation. *Biopolymers: Original Research on Biomolecules*, 67(1):1–9, 2002.

[11] Melisew Tadele Alula, Zebasil Tassew Mengesha, and Ellen Mwenesongole. Advances in surface-enhanced raman spectroscopy for analysis of pharmaceuticals: A review. *Vibrational Spectroscopy*, 98:50–63, 2018.

[12] Zoran V Popović, Z Dohčević-Mitrović, M Šćepanović, M Grujić-Brojčin, and S Aškrabić. Raman scattering on nanomaterials and nanostructures. *Annalen der Physik*, 523(1-2):62–74, 2011.

[13] Onofrio M Marago, Philip H Jones, Pietro G Gucciardi, Giovanni Volpe, and Andrea C Ferrari. Optical trapping and manipulation of nanostructures. *Nature Nanotechnology*, 8(11):807–819, 2013.

[14] Eun-Soo Kwak, Tiberiu-Dan Onuta, Dragos Amarie, Radislav Potyrailo, Barry Stein, Stephen C Jacobson, WL Schaich, and Bogdan Dragnea. Optical trapping

with integrated near-field apertures. *The Journal of Physical Chemistry B*, 108(36):13607–13612, 2004.

[15] Stefan A Maier et al. *Plasmonics: fundamentals and applications*, volume 1. Springer, 2007.

[16] Raju Regmi, Ahmed A Al Balushi, Hervé Rigneault, Reuven Gordon, and Jérôme Wenger. Nanoscale volume confinement and fluorescence enhancement with double nanohole aperture. *Scientific Reports*, 5(1):15852, 2015.

[17] Steven Jones, Ahmed A Al Balushi, and Reuven Gordon. Raman spectroscopy of single nanoparticles in a double-nanohole optical tweezer system. *Journal of Optics*, 17(10):102001, 2015.

[18] Hao Zhang, Parinaz Moazzezi, Juanjuan Ren, Brett Henderson, Cristina Cordoba, Vishal Yeddu, Arthur M Blackburn, Makhsud I Saidaminov, Irina Paci, Stephen Hughes, et al. Coupling perovskite quantum dot pairs in solution using a nanoplasmonic assembly. *Nano Letters*, 22(13):5287–5293, 2022.

[19] Amirhossein Alizadehkhaledi, Adriaan L Frencken, Mohsen Kamandar Dezfouli, Stephen Hughes, Frank CJM van Veggel, and Reuven Gordon. Cascaded plasmon-enhanced emission from a single upconverting nanocrystal. *ACS Photonics*, 6(5):1125–1131, 2019.

[20] Elham Babaei, Ghazal Hajisalem, Shohei Iwamoto, Burak Kaynak, Pemra Doruker, Mohsin M Naqvi, Janet Kumita, Feng-Yu Wang, Jhih-Hong Cheng, Che-Min Wu, et al. Extraordinary acoustic raman spectroscopy of pr65. In *2021 IEEE 16th Nanotechnology Materials and Devices Conference (NMDC)*, pages 1–4. IEEE, 2021.

[21] S Sohila, M Rajalakshmi, Chanchal Ghosh, AK Arora, and C Muthamizhchelvan. Optical and raman scattering studies on sns nanoparticles. *Journal of Alloys and Compounds*, 509(19):5843–5847, 2011.

[22] Cedrik Meier, Stephan Lüttjohann, Vasyl G Kravets, Hermann Nienhaus, Axel Lorke, and Hartmut Wiggers. Raman properties of silicon nanoparticles. *Physica E: Low-dimensional Systems and Nanostructures*, 32(1-2):155–158, 2006.

[23] Gitti L Frey, Reshef Tenne, Manyalibo J Matthews, MS Dresselhaus, and G Dresselhaus. Raman and resonance raman investigation of mos2 nanoparticles. *Physical Review B*, 60(4):2883, 1999.

[24] Paul L Stiles, Jon A Dieringer, Nilam C Shah, and Richard P Van Duyne. Surface-enhanced raman spectroscopy. *Annual Review of Analytical Chemistry*, 1:601–626, 2008.

[25] Prabhat Verma. Tip-enhanced raman spectroscopy: technique and recent advances. *Chemical Reviews*, 117(9):6447–6466, 2017.

[26] Nadia Djaker, Richard Hostein, Eloïse Devaux, Thomas W Ebbesen, Hervé Rigneault, and Jérôme Wenger. Surface enhanced raman scattering on a single nanometric aperture. *The Journal of Physical Chemistry C*, 114(39):16250–16256, 2010.

[27] L Rkiouak, MJ Tang, JCJ Camp, J McGregor, IM Watson, RA Cox, M Kalberer, AD Ward, and FD Pope. Optical trapping and raman spectroscopy of solid particles. *Physical Chemistry Chemical Physics*, 16(23):11426–11434, 2014.

[28] Behnam Khosravi and Reuven Gordon. Reflection mode optical trapping using polarization symmetry breaking from tilted double nanoholes. *Optics Express*, 31(2):2621–2627, 2023.

[29] Behnam Khosravi and Reuven Gordon. Accessible double nanohole raman tweezer analysis of single nanoparticles. *The Journal of Physical Chemistry C*, 128(36):15048–15053, 2024.

[30] Reuven Gordon and Behnam Khosravi. Polarization selective reflection geometry trapping of nanoparticles, February 15 2024. US Patent Application 18/448,082.

[31] Xiang Wang, Sheng-Chao Huang, Shu Hu, Sen Yan, and Bin Ren. Fundamental understanding and applications of plasmon-enhanced raman spectroscopy. *Nature Reviews Physics*, 2(5):253–271, 2020.

[32] Yong Chen and Hai Ming. Review of surface plasmon resonance and localized surface plasmon resonance sensor. *Photonic Sensors*, 2:37–49, 2012.

[33] Jiri Homola, Sinclair S Yee, and Gunter Gauglitz. Surface plasmon resonance sensors. *Sensors and Actuators B: Chemical*, 54(1-2):3–15, 1999.

[34] Min-Ki Kwon, Ja-Yeon Kim, Baek-Hyun Kim, Il-Kyu Park, Chu-Young Cho, Clare Chisu Byeon, and Seong-Ju Park. Surface-plasmon-enhanced light-emitting diodes. *Advanced Materials*, 20(7):1253–1257, 2008.

[35] Xuefeng Gu, Teng Qiu, Wenjun Zhang, and Paul K Chu. Light-emitting diodes enhanced by localized surface plasmon resonance. *Nanoscale Research Letters*, 6:1–12, 2011.

[36] Jeremy W Jarrett, Tian Zhao, Jeffrey S Johnson, and Kenneth L Knappenberger Jr. Investigating plasmonic structure-dependent light amplification and

electronic dynamics using advances in nonlinear optical microscopy. *The Journal of Physical Chemistry C*, 119(28):15779–15800, 2015.

[37] Shaoxin Shen, Yue Zeng, Zehuan Zheng, Renxian Gao, Guoya Sun, and Zhilin Yang. Nonlinear light amplification via 3d plasmonic nanocavities. *Optics Express*, 30(2):2610–2625, 2022.

[38] Argishti Melikyan, Luca Alloatti, Alban Muslija, David Hillerkuss, Philipp C Schindler, J Li, Robert Palmer, Dietmar Korn, Sascha Muehlbrandt, Dries Van Thourhout, et al. High-speed plasmonic phase modulators. *Nature Photonics*, 8(3):229–233, 2014.

[39] Masafumi Ayata, Yuriy Fedoryshyn, Wolfgang Heni, Benedikt Baeuerle, Arne Josten, Marco Zahner, Ueli Koch, Yannick Salamin, Claudia Hoessbacher, Christian Haffner, et al. High-speed plasmonic modulator in a single metal layer. *Science*, 358(6363):630–632, 2017.

[40] Hans Albrecht Bethe. Theory of diffraction by small holes. *Physical Review*, 66(7-8):163, 1944.

[41] Thomas W Ebbesen, Henri J Lezec, HF Ghaemi, Tineke Thio, and Peter A Wolff. Extraordinary optical transmission through sub-wavelength hole arrays. *Nature*, 391(6668):667–669, 1998.

[42] Arthur Ashkin, James M Dziedzic, John E Bjorkholm, and Steven Chu. Observation of a single-beam gradient force optical trap for dielectric particles. *Optics Letters*, 11(5):288–290, 1986.

[43] Arthur Ashkin and James M Dziedzic. Optical trapping and manipulation of viruses and bacteria. *Science*, 235(4795):1517–1520, 1987.

[44] Chuchuan Hong and Justus C Ndukaife. Scalable trapping of single nanosized extracellular vesicles using plasmonics. *arXiv preprint arXiv:2302.07370*, 2023.

[45] William L Barnes, Alain Dereux, and Thomas W Ebbesen. Surface plasmon subwavelength optics. *Nature*, 424(6950):824–830, 2003.

[46] Rana Sadaf Anwar, Huansheng Ning, and Lingfeng Mao. Recent advancements in surface plasmon polaritons-plasmonics in subwavelength structures in microwave and terahertz regimes. *Digital Communications and Networks*, 4(4):244–257, 2018.

[47] Tineke Thio, KM Pellerin, RA Linke, HJ Lezec, and TW Ebbesen. Enhanced light transmission through a single subwavelength aperture. *Optics Letters*, 26(24):1972–1974, 2001.

[48] Fanxin Liu, Boxiang Song, Guangxu Su, Owen Liang, Peng Zhan, Han Wang, Wei Wu, Yahong Xie, and Zhenlin Wang. Sculpting extreme electromagnetic field enhancement in free space for molecule sensing. *Small*, 14(33):1801146, 2018.

[49] Ahmed A Al Balushi, Ana Zehtabi-Oskuie, and Reuven Gordon. Observing single protein binding by optical transmission through a double nanohole aperture in a metal film. *Biomedical Optics Express*, 4(9):1504–1511, 2013.

[50] Sergei G Romanov, Alexander V Korovin, Alois Regensburger, and Ulf Peschel. Hybrid colloidal plasmonic-photonic crystals. *Advanced Materials*, 23(22-23):2515–2533, 2011.

[51] Harry A Atwater and Albert Polman. Plasmonics for improved photovoltaic devices. *Nature Materials*, 9(3):205–213, 2010.

[52] Xiaohua Huang, Prashant K Jain, Ivan H El-Sayed, and Mostafa A El-Sayed. Plasmonic photothermal therapy (pptt) using gold nanoparticles. *Lasers in Medical Science*, 23:217–228, 2008.

[53] Paul R West, Satoshi Ishii, Gururaj V Naik, Naresh K Emani, Vladimir M Shalaev, and Alexandra Boltasseva. Searching for better plasmonic materials. *Laser & photonics reviews*, 4(6):795–808, 2010.

[54] Martin G Blaber, Matthew D Arnold, and Michael J Ford. Search for the ideal plasmonic nanoshell: the effects of surface scattering and alternatives to gold and silver. *The Journal of Physical Chemistry C*, 113(8):3041–3045, 2009.

[55] Rituraj Borah, Rajeshreddy Ninakanti, Sara Bals, and Sammy W Verbruggen. Plasmon resonance of gold and silver nanoparticle arrays in the kretschmann (attenuated total reflectance) vs. direct incidence configuration. *Scientific Reports*, 12(1):15738, 2022.

[56] Alexandre Vial, Anne-Sophie Grimault, Demetrio Macías, Dominique Barchiesi, and Marc Lamy De La Chapelle. Improved analytical fit of gold dispersion: Application to the modeling of extinction spectra with a finite-difference time-domain method. *Physical Review B*, 71(8):085416, 2005.

[57] Svetlana V Boriskina, Thomas Alan Cooper, Lingping Zeng, George Ni, Jonathan K Tong, Yoichiro Tsurimaki, Yi Huang, Laureen Meroueh, Gerald Mahan, and Gang Chen. Losses in plasmonics: from mitigating energy dissipation to embracing loss-enabled functionalities. *Advances in Optics and Photonics*, 9(4):775–827, 2017.

[58] JR Sambles, GW Bradbery, and Fuzi Yang. Optical excitation of surface plasmons: an introduction. *Contemporary Physics*, 32(3):173–183, 1991.

[59] Robert L Olmon, Brian Slovick, Timothy W Johnson, David Shelton, Sang-Hyun Oh, Glenn D Boreman, and Markus B Raschke. Optical dielectric function of gold. *Physical Review B*, 86(23):235147, 2012.

[60] Erwin Kretschmann and Heinz Raether. Radiative decay of non radiative surface plasmons excited by light. *Zeitschrift für Naturforschung A*, 23(12):2135–2136, 1968.

[61] Andreas Otto. Excitation of nonradiative surface plasma waves in silver by the method of frustrated total reflection. *Zeitschrift für Physik A Hadrons and Nuclei*, 216(4):398–410, 1968.

[62] Jana Olson, Sergio Dominguez-Medina, Anneli Hoggard, Lin-Yung Wang, Wei-Shun Chang, and Stephan Link. Optical characterization of single plasmonic nanoparticles. *Chemical Society Reviews*, 44(1):40–57, 2015.

[63] Arafeh Bigdeli, Forough Ghasemi, Hamed Golmohammadi, Samira Abbasi-Moayed, M Amin Farahmand Nejad, Nafiseh Fahimi-Kashani, Somayeh Jafarinejad, Maryam Shahrajabian, and M Reza Hormozi-Nezhad. Nanoparticle-based optical sensor arrays. *Nanoscale*, 9(43):16546–16563, 2017.

[64] Hong Wei, Deng Pan, Shunping Zhang, Zhipeng Li, Qiang Li, Ning Liu, Wenhui Wang, and Hongxing Xu. Plasmon waveguiding in nanowires. *Chemical Reviews*, 118(6):2882–2926, 2018.

[65] Xin Guo, Yibin Ying, and Limin Tong. Photonic nanowires: from subwavelength waveguides to optical sensors. *Accounts of Chemical Research*, 47(2):656–666, 2014.

[66] Si Hoon Lee, Kyle C Bantz, Nathan C Lindquist, Sang-Hyun Oh, and Christy L Haynes. Self-assembled plasmonic nanohole arrays. *Langmuir*, 25(23):13685–13693, 2009.

[67] Syu-Cing Ma, Rohit Gupta, Neil Adrian P Ondevilla, Kuntal Barman, Liang-Yun Lee, Hsien-Chang Chang, and Jian-Jang Huang. Voltage-modulated surface plasmon resonance biosensors integrated with gold nanohole arrays. *Biomedical Optics Express*, 14(1):182–193, 2022.

[68] Yang Zhao and Andrea Alù. Manipulating light polarization with ultrathin plasmonic metasurfaces. *Physical Review B*, 84(20):205428, 2011.

[69] Gururaj V Naik, Vladimir M Shalaev, and Alexandra Boltasseva. Alternative plasmonic materials: beyond gold and silver. *Advanced Materials*, 25(24):3264–3294, 2013.

[70] Urcan Guler, Vladimir M Shalaev, and Alexandra Boltasseva. Nanoparticle plasmonics: going practical with transition metal nitrides. *Materials Today*, 18(4):227–237, 2015.

[71] Matthew Pelton, Javier Aizpurua, and Garnett Bryant. Metal-nanoparticle plasmonics. *Laser & Photonics Reviews*, 2(3):136–159, 2008.

[72] Jiapeng Zheng, Xizhe Cheng, Han Zhang, Xiaopeng Bai, Ruoqi Ai, Lei Shao, and Jianfang Wang. Gold nanorods: the most versatile plasmonic nanoparticles. *Chemical Reviews*, 121(21):13342–13453, 2021.

[73] Matthew E Stewart, Christopher R Anderton, Lucas B Thompson, Joana Maria, Stephen K Gray, John A Rogers, and Ralph G Nuzzo. Nanostructured plasmonic sensors. *Chemical Reviews*, 108(2):494–521, 2008.

[74] Qilin Duan, Yineng Liu, Shanshan Chang, Huanyang Chen, and Jin-hui Chen. Surface plasmonic sensors: Sensing mechanism and recent applications. *Sensors*, 21(16):5262, 2021.

[75] Nidhi Nath and Ashutosh Chilkoti. A colorimetric gold nanoparticle sensor to interrogate biomolecular interactions in real time on a surface. *Analytical Chemistry*, 74(3):504–509, 2002.

[76] Sebastian Schlücker. Surface-enhanced raman spectroscopy: Concepts and chemical applications. *Angewandte Chemie International Edition*, 53(19):4756–4795, 2014.

[77] Matthew J Horton, Oluwafemi S Ojambati, Rohit Chikkaraddy, William M Deacon, Nuttawut Kongsuwan, Angela Demetriadou, Ortwin Hess, and Jeremy J Baumberg. Nanoscopy through a plasmonic nanolens. *Proceedings of the National Academy of Sciences*, 117(5):2275–2281, 2020.

[78] Skyler Wheaton and Reuven Gordon. Molecular weight characterization of single globular proteins using optical nanotweezers. *Analyst*, 140(14):4799–4803, 2015.

[79] Ana Zehtabi-Oskuie, Hao Jiang, Bryce R Cyr, Douglas W Rennehan, Ahmed A Al-Balushi, and Reuven Gordon. Double nanohole optical trapping: dynamics and protein-antibody co-trapping. *Lab on a Chip*, 13(13):2563–2568, 2013.

[80] Daehan Yoo, Kargal L Gurunatha, Han-Kyu Choi, Daniel A Mohr, Christopher T Ertsgaard, Reuven Gordon, and Sang-Hyun Oh. Low-power optical trapping of nanoparticles and proteins with resonant coaxial nanoaperture using 10 nm gap. *Nano Letters*, 18(6):3637–3642, 2018.

[81] Ahmad Reza Hajiaboli, Bo Cui, M Kahrizi, and Vo-Van Truong. Optical properties of thick metal nanohole arrays fabricated by electron-beam and nanosphere lithography. *Physica Status Solidi (a)*, 206(5):976–979, 2009.

[82] Dayang Wang and Helmuth Möhwald. Template-directed colloidal self-assembly–the route to 'top-down'nanochemical engineering. *Journal of Materials Chemistry*, 14(4):459–468, 2004.

[83] MA Verschuuren, MJA De Dood, D Stolwijk, A Polman, et al. Optical properties of high-quality nanohole arrays in gold made using soft-nanoimprint lithography. *MRS Communications*, 5(4):547–553, 2015.

[84] Adarsh Lalitha Ravindranath, Mirali Seyed Shariatdoust, Samuel Mathew, and Reuven Gordon. Colloidal lithography double-nanohole optical trapping of nanoparticles and proteins. *Optics Express*, 27(11):16184–16194, 2019.

[85] Yuanyuan Chen, Abhay Kotnala, Li Yu, Jiasen Zhang, and Reuven Gordon. Wedge and gap plasmonic resonances in double nanoholes. *Optics Express*, 23(23):30227–30236, 2015.

[86] Edward D Palik. *Handbook of optical constants of solids*, volume 3. Academic Press, 1998.

[87] Ana Zehtabi-Oskuie, Jarrah Gerald Bergeron, and Reuven Gordon. Flow-dependent double-nanohole optical trapping of 20 nm polystyrene nanospheres. *Scientific Reports*, 2:966, 2012.

[88] Noa Hacohen, Candice JX Ip, and Reuven Gordon. Analysis of egg white protein composition with double nanohole optical tweezers. *ACS Omega*, 3(5):5266–5272, 2018.

[89] Matthew Peters, Sina Halvaei, Tianyu Zhao, Annie Yang-Schulz, Karla C Williams, and Reuven Gordon. Classification of single extracellular vesicles in a double nanohole optical tweezer for cancer detection. *Journal of Physics: Photonics*, 6(3):035017, 2024.

[90] Matthew Peters, Tianyu Zhao, Sherin George, Viet Giang Truong, Síle Nic Chormaic, Cuifeng Ying, René A Nome, and Reuven Gordon. Energy landscape of conformational changes for a single unmodified protein. *npj Biosensing*, 1(1):14, 2024.

[91] Steven Jones. *Characterization of single nanoparticles*. PhD thesis, University of Victoria, 2016.

[92] Yanxiao Feng, Yuechuan Zhang, Cuifeng Ying, Deqiang Wang, and Chunlei Du. Nanopore-based fourth-generation dna sequencing technology. *Genomics, Proteomics and Bioinformatics*, 13(1):4–16, 2015.

[93] Maria Steinke, Florian Zunhammer, Elisavet I Chatzopoulou, Henrik Teller, Karin Schütze, Heike Walles, Joachim O Rädler, and Cordula Grüttner. Rapid analysis of cell–nanoparticle interactions using single-cell raman trapping microscopy. *Angewandte Chemie International Edition*, 57(18):4946–4950, 2018.

[94] Jianwei Yan, Yang Chen, Xiaowu Wang, Ying Fu, Juxiang Wang, Jia Sun, Guozhang Dai, Shaohua Tao, and Yongli Gao. High-performance solar-blind sno 2 nanowire photodetectors assembled using optical tweezers. *Nanoscale*, 11(5):2162–2169, 2019.

[95] Mark Daly, Marios Sergides, and Síle Nic Chormaic. Optical trapping and manipulation of micrometer and submicrometer particles. *Laser & Photonics Reviews*, 9(3):309–329, 2015.

[96] Yuquan Zhang, Changjun Min, Xiujie Dou, Xianyou Wang, Hendrik Paul Urbach, Michael G Somekh, and Xiaocong Yuan. Plasmonic tweezers: for nanoscale optical trapping and beyond. *Light: Science & Applications*, 10(1):59, 2021.

[97] Quanbo Jiang, Jean-Benoît Claude, and Jérôme Wenger. Plasmonic nano-optical trap stiffness measurements and design optimization. *Nanoscale*, 13(7):4188–4194, 2021.

[98] Yuanjie Pang and Reuven Gordon. Optical trapping of 12 nm dielectric spheres using double-nanoholes in a gold film. *Nano Letters*, 11(9):3763–3767, 2011.

[99] Yuanjie Pang and Reuven Gordon. Optical trapping of a single protein. *Nano Letters*, 12(1):402–406, 2012.

[100] Sarp Kerman, Chang Chen, Yi Li, Wim Van Roy, Liesbet Lagae, and Pol Van Dorpe. Raman fingerprinting of single dielectric nanoparticles in plasmonic nanopores. *Nanoscale*, 7(44):18612–18618, 2015.

[101] Hyun Chul Choi, Young Mee Jung, and Seung Bin Kim. Size effects in the raman spectra of tio2 nanoparticles. *Vibrational Spectroscopy*, 37(1):33–38, 2005.

[102] I Lorite, JJ Romero, and JF Fernández. Effects of the agglomeration state on the raman properties of co3o4 nanoparticles. *Journal of Raman Spectroscopy*, 43(10):1443–1448, 2012.

[103] Nathan C Lindquist, Carlos Diego L de Albuquerque, Regivaldo G Sobral-Filho, Irina Paci, and Alexandre G Brolo. High-speed imaging of surface-enhanced raman scattering fluctuations from individual nanoparticles. *Nature Nanotechnology*, 14(10):981–987, 2019.

[104] Carlos Diego L De Albuquerque, Kallai M Hokanson, Sarah R Thorud, Regivaldo G Sobral-Filho, Nathan C Lindquist, and Alexandre G Brolo. Dynamic imaging of multiple sers hotspots on single nanoparticles. *ACS Photonics*, 7(2):434–443, 2020.

[105] Yue Bing Zheng, John L Payton, Tze-Bin Song, Bala Krishna Pathem, Yuxi Zhao, Hong Ma, Yang Yang, Lasse Jensen, Alex K-Y Jen, and Paul S Weiss. Surface-enhanced raman spectroscopy to probe photoreaction pathways and kinetics of isolated reactants on surfaces: flat versus curved substrates. *Nano Letters*, 12(10):5362–5368, 2012.

[106] Dongdong Lin, Zilong Wu, Shujie Li, Wenqi Zhao, Chongjun Ma, Jie Wang, Zuimin Jiang, Zhenyang Zhong, Yuebing Zheng, and Xinju Yang. Large-area au-nanoparticle-functionalized si nanorod arrays for spatially uniform surface-enhanced raman spectroscopy. *ACS Nano*, 11(2):1478–1487, 2017.

[107] Diego P Dos Santos, Marcia LA Temperini, and Alexandre G Brolo. Intensity fluctuations in single-molecule surface-enhanced raman scattering. *Accounts of Chemical Research*, 52(2):456–464, 2019.

[108] Nathan C Lindquist, Ariadne T Bido, and Alexandre G Brolo. Single-molecule sers hotspot dynamics in both dry and aqueous environments. *The Journal of Physical Chemistry C*, 126(16):7117–7126, 2022.

[109] Cuifeng Ying, Edona Karakaci, Esteban Bermudez-Urena, Alessandro Ianiro, Ceri Foster, Saurabh Awasthi, Anirvan Guha, Louise Bryan, Jonathan List, Sandor Balog, Guillermo P Acuna, Reuven Gordon, and Michael Mayer. Watching single unmodified enzymes at work. *arXiv preprint arXiv:2107.06407 physics.bio-ph*, 13 July 2021, https://arxiv.org/abs/2107.06407, accessed 2024-07-25.

[110] Katsuhiro Ajito and Keiichi Torimitsu. Single nanoparticle trapping using a raman tweezers microscope. *Applied Spectroscopy*, 56(4):541–544, 2002.

[111] Charles J Choi, Zhida Xu, Hsin-Yu Wu, Gang Logan Liu, and Brian T Cunningham. Surface-enhanced raman nanodomes. *Nanotechnology*, 21(41):415301, 2010.

[112] Jwa-Min Nam, Jeong-Wook Oh, Haemi Lee, and Yung Doug Suh. Plasmonic nanogap-enhanced raman scattering with nanoparticles. *Accounts of Chemical Research*, 49(12):2746–2755, 2016.

[113] Kevin G Stamplecoskie, Juan C Scaiano, Vidhu S Tiwari, and Hanan Anis. Optimal size of silver nanoparticles for surface-enhanced raman spectroscopy. *The Journal of Physical Chemistry C*, 115(5):1403–1409, 2011.

[114] Jian Feng Li, Yi Fan Huang, Yong Ding, Zhi Lin Yang, Song Bo Li, Xiao Shun Zhou, Feng Ru Fan, Wei Zhang, Zhi You Zhou, De Yin Wu, et al. Shell-isolated nanoparticle-enhanced raman spectroscopy. *Nature*, 464(7287):392–395, 2010.

[115] Shuming Nie and Steven R Emory. Probing single molecules and single nanoparticles by surface-enhanced raman scattering. *Science*, 275(5303):1102–1106, 1997.

[116] Christopher T Ertsgaard, Nathan J Wittenberg, Daniel J Klemme, Avijit Barik, Wei-Chuan Shih, and Sang-Hyun Oh. Integrated nanogap platform for sub-volt dielectrophoretic trapping and real-time raman imaging of biological nanoparticles. *Nano Letters*, 18(9):5946–5953, 2018.

[117] H Yoshikawa, T Adachi, G Sazaki, T Matsui, K Nakajima, and Hiroshi Masuhara. Surface-enhanced hyper-raman spectroscopy using optical trapping of

silver nanoparticles for molecular detection in solution. *Journal of Optics A: Pure and Applied Optics*, 9(8):S164, 2007.

[118] Emma Vander Ende, Marc R Bourgeois, Anne-Isabelle Henry, Jorge L Chávez, Rachel Krabacher, George C Schatz, and Richard P Van Duyne. Physicochemical trapping of neurotransmitters in polymer-mediated gold nanoparticle aggregates for surface-enhanced raman spectroscopy. *Analytical Chemistry*, 91(15):9554–9562, 2019.

[119] E Messina, E Cavallaro, Adriano Cacciola, Rosalba Saija, Ferdinando Borghese, Paolo Denti, B Fazio, Cristiano D'Andrea, PG Gucciardi, MA Iati, et al. Manipulation and raman spectroscopy with optically trapped metal nanoparticles obtained by pulsed laser ablation in liquids. *The Journal of Physical Chemistry C*, 115(12):5115–5122, 2011.

[120] Mohammadali Tabatabaei, Mohamadreza Najiminaini, Kieffer Davieau, Bozena Kaminska, Mahi R Singh, Jeffrey JL Carson, and François Lagugné-Labarthet. Tunable 3d plasmonic cavity nanosensors for surface-enhanced raman spectroscopy with sub-femtomolar limit of detection. *ACS Photonics*, 2(6):752–759, 2015.

[121] Ariadne T Bido, Britta G Nordberg, Marit A Engevik, Nathan C Lindquist, and Alexandre G Brolo. High-speed fluctuations in surface-enhanced raman scattering intensities from various nanostructures. *Applied Spectroscopy*, 74(11):1398–1406, 2020.

[122] Wenqi Zhu and Kenneth B Crozier. Quantum mechanical limit to plasmonic enhancement as observed by surface-enhanced raman scattering. *Nature Communications*, 5(1):5228, 2014.

[123] Michael P Cecchini, Aeneas Wiener, Vladimir A Turek, Hyangh Chon, Sangyeop Lee, Aleksandar P Ivanov, David W McComb, Jaebum Choo, Tim Albrecht, Stefan A Maier, et al. Rapid ultrasensitive single particle surface-enhanced raman spectroscopy using metallic nanopores. *Nano Letters*, 13(10):4602–4609, 2013.

[124] Kenneth B Crozier, Wenqi Zhu, Dongxing Wang, Shiyun Lin, Michael D Best, and Jon P Camden. Plasmonics for surface enhanced raman scattering: Nanoantennas for single molecules. *IEEE Journal of Selected Topics in Quantum Electronics*, 20(3):152–162, 2013.

[125] Shiyun Lin, Wenqi Zhu, Yuhang Jin, and Kenneth B Crozier. Surface-enhanced raman scattering with ag nanoparticles optically trapped by a photonic crystal cavity. *Nano Letters*, 13(2):559–563, 2013.

[126] Matthew D King, Sushil Khadka, Gary A Craig, and Michael D Mason. Effect of local heating on the sers efficiency of optically trapped prismatic nanoparticles. *The Journal of Physical Chemistry C*, 112(31):11751–11757, 2008.

[127] Jared Houghtaling, Cuifeng Ying, Olivia M Eggenberger, Aziz Fennouri, Santoshi Nandivada, Mitu Acharjee, Jiali Li, Adam R Hall, and Michael Mayer. Estimation of shape, volume, and dipole moment of individual proteins freely transiting a synthetic nanopore. *ACS Nano*, 13(5):5231–5242, 2019.

[128] Hao-Wei Guo, Yang-Jun Cui, Yu-Zhe Zhang, Yun-Long Wang, Bao-Wang Su, Wen-yuan Zhou, Jian-Guo Tian, Cui-Feng Ying, and Zhi-Bo Liu. Stable nanopores in two-dimensional materials for ion conductivity devices and biosensors. *ACS Applied Nano Materials*, 5(3):3611–3618, 2022.

[129] Elham Hosseini Toodeshki, Adriaan L Frencken, Frank CJM van Veggel, and Reuven Gordon. Thermometric analysis of nanoaperture-trapped erbium-containing nanocrystals. *ACS Photonics*, 11(4):1390–1395, 2024.

[130] Zohreh Sharifi, Michael Dobinson, Ghazal Hajisalem, Mirali Seyed Shariatdoust, Adriaan L Frencken, Frank CJM van Veggel, and Reuven Gordon. Isolating and enhancing single-photon emitters for 1550 nm quantum light sources using double nanohole optical tweezers. *The Journal of Chemical Physics*, 154(18), 2021.

[131] Adriaan L Frencken, Michael Dobinson, Zohreh Sharifi, Elham Hosseini Toodeshki, Reuven Gordon, and Frank CJM van Veggel. Photochemical anchoring of singly er3+ ion-doped nayf4 nanoparticles for scalable fabrication of single-photon emitting devices: Implications for quantum light sources in the telecom window. *ACS Applied Nano Materials*, 6(6):4398–4405, 2023.

[132] Chuchuan Hong, Sen Yang, and Justus C Ndukaife. Stand-off trapping and manipulation of sub-10 nm objects and biomolecules using opto-thermo-electrohydrodynamic tweezers. *Nature Nanotechnology*, 15(11):908–913, 2020.

[133] Russell A Jensen, I-Chun Huang, Ou Chen, Jennifer T Choy, Thomas S Bischof, Marko Loncar, and Moungi G Bawendi. Optical trapping and two-photon excitation of colloidal quantum dots using bowtie apertures. *ACS Photonics*, 3(3):423–427, 2016.

[134] Muhammad Usman Raza, Sai Santosh Sasank Peri, Liang-Chieh Ma, Samir M Iqbal, and George Alexandrakis. Self-induced back action actuated nanopore electrophoresis (sane). *Nanotechnology*, 29(43):435501, 2018.

[135] Lamyaa M Almehmadi, Stephanie M Curley, Natalya A Tokranova, Scott A Tenenbaum, and Igor K Lednev. Surface enhanced raman spectroscopy for single molecule protein detection. *Scientific Reports*, 9(1):12356, 2019.

[136] Yuxuan Qiu, Cuifang Kuang, Xu Liu, and Longhua Tang. Single-molecule surface-enhanced raman spectroscopy. *Sensors*, 22(13):4889, 2022.

[137] Daniel V Verschueren, Magnus P Jonsson, and Cees Dekker. Temperature dependence of dna translocations through solid-state nanopores. *Nanotechnology*, 26(23):234004, 2015.

[138] Chia-Chi Huang, Zi-Han Hsu, and Yen-Shi Lai. Raman spectroscopy for virus detection and the implementation of unorthodox food safety. *Trends in Food Science & Technology*, 116:525–532, 2021.

[139] Jian Ma, XiongJie Ning, YuanHao Lou, Dan Wu, QiuHong Min, YiRui Wang, Quan Zhang, and YuanJie Pang. Raman spectroscopy of optical-trapped single particle using bull's eye nanostructure. *Optics Letters*, 48(5):1204–1207, 2023.

[140] Andrea Orlando, Filippo Franceschini, Cristian Muscas, Solomiya Pidkova, Mattia Bartoli, Massimo Rovere, and Alberto Tagliaferro. A comprehensive review on raman spectroscopy applications. *Chemosensors*, 9(9):262, 2021.

[141] EC Le Ru, M Meyer, E Blackie, and PG Etchegoin. Advanced aspects of electromagnetic sers enhancement factors at a hot spot. *Journal of Raman Spectroscopy*, 39(9):1127–1134, 2008.

[142] Eric C Le Ru and Pablo G Etchegoin. Quantifying sers enhancements. *MRS Bulletin*, 38(8):631–640, 2013.

[143] Jiang, Ken Bosnick, Mathieu Maillard, and Louis Brus. Single molecule raman spectroscopy at the junctions of large ag nanocrystals, 2003.

[144] Eric C Le Ru and Pablo G Etchegoin. Single-molecule surface-enhanced raman spectroscopy. *Annual Review of Physical Chemistry*, 63(1):65–87, 2012.

[145] Gustavo de Miguel, Giuseppe Vicidomini, Benjamin Harke, and Alberto Diaspro. Chapter 8 - linewidth and writing resolution. In Tommaso Baldacchini, editor, *Three-Dimensional Microfabrication Using Two-photon Polymerization*, Micro and Nano Technologies, pages 190–220. William Andrew Publishing, Oxford, 2016.

[146] Granite. Laser Spot Size in a Microscope | Airy Disk | Raman & Fluorescence.

[147] Peter B Johnson and R-WJPrB Christy. Optical constants of the noble metals. *Physical Review B*, 6(12):4370, 1972.

[148] Ghazal Hajisalem, Elham Babaei, Michael Dobinson, Shohei Iwamoto, Zohreh Sharifi, Jon Eby, Marie Synakewicz, Laura S Itzhaki, and Reuven Gordon. Accessible high-performance double nanohole tweezers. *Optics Express*, 30(3):3760–3769, 2022.

[149] Tiberiu-Dan Onuta, Matthias Waegele, Christopher C DuFort, William L Schaich, and Bogdan Dragnea. Optical field enhancement at cusps between adjacent nanoapertures. *Nano letters*, 7(3):557–564, 2007.

[150] Michael Dobinson. *A route to erbium-doped nanocrystals as a single photon source using double nanohole optical tweezers*. PhD thesis, University of Victoria, 2022.

[151] Matthew Peters, Declan McIntosh, Alexandra Branzan Albu, Cuifeng Ying, and Reuven Gordon. Label-free tracking of proteins through plasmon-enhanced interference. *ACS Nanoscience Au*, 4(1):69–75, 2023.

[152] Rajini P Antony, Arup Dasgupta, Sudipta Mahana, D Topwal, Tom Mathews, and Sandip Dhara. Resonance raman spectroscopic study for radial vibrational modes in ultra-thin walled tio2 nanotubes. *Journal of Raman Spectroscopy*, 46(2):231–235, 2015.

[153] H Tang, K Prasad, R Sanjines, PE Schmid, and F Levy. Electrical and optical properties of tio2 anatase thin films. *Journal of Applied Physics*, 75(4):2042–2047, 1994.

[154] Johann Berthelot, Srdjan S Aćimović, Mathieu L Juan, Mark P Kreuzer, Jan Renger, and Romain Quidant. Three-dimensional manipulation with scanning near-field optical nanotweezers. *Nature Nanotechnology*, 9(4):295–299, 2014.

[155] Mohamed M Matoug and Reuven Gordon. Crude oil asphaltenes studied by terahertz spectroscopy. *ACS Omega*, 3(3):3406–3412, 2018.

[156] Thomas Nagel, Eva Ehrentreich-Förster, Mahavir Singh, Katrin Schmitt, Albrecht Brandenburg, Alexander Berka, and Frank F Bier. Direct detection of tuberculosis infection in blood serum using three optical label-free approaches. *Sensors and Actuators B: Chemical*, 129(2):934–940, 2008.

[157] Sai Santosh Sasank Peri, Manoj K Sabnani, Muhammad Usman Raza, Soroush Ghaffari, Susanne Gimlin, Debra D Wawro, Jung Soo Lee, Min Jun Kim, Jon Weidanz, and George Alexandrakis. Detection of specific antibody-ligand interactions with a self-induced back-action actuated nanopore electrophoresis sensor. *Nanotechnology*, 31(8):085502, 2019.

[158] Daniel Verschueren, Xin Shi, and Cees Dekker. Nano-optical tweezing of single proteins in plasmonic nanopores. *Small Methods*, 3(5):1800465, 2019.

[159] Zhe Xu, Wuzhou Song, and Kenneth B Crozier. Optical trapping of nanoparticles using all-silicon nanoantennas. *ACS Photonics*, 5(12):4993–5001, 2018.

[160] Zhe Xu, Wuzhou Song, and Kenneth B Crozier. Direct particle tracking observation and brownian dynamics simulations of a single nanoparticle optically trapped by a plasmonic nanoaperture. *ACS Photonics*, 5(7):2850–2859, 2018.

[161] Quanbo Jiang, Benoit Rogez, Jean-Benoît Claude, Guillaume Baffou, and Jérôme Wenger. Temperature measurement in plasmonic nanoapertures used for optical trapping. *ACS Photonics*, 6(7):1763–1773, 2019.

[162] Quanbo Jiang, Benoît Rogez, Jean-Benoît Claude, Antonin Moreau, Julien Lumeau, Guillaume Baffou, and Jérôme Wenger. Adhesion layer influence on controlling the local temperature in plasmonic gold nanoholes. *Nanoscale*, 12(4):2524–2531, 2020.

[163] Quanbo Jiang, Benoît Rogez, Jean-Benoît Claude, Guillaume Baffou, and Jérôme Wenger. Quantifying the role of the surfactant and the thermophoretic force in plasmonic nano-optical trapping. *Nano Letters*, 20(12):8811–8817, 2020.